Directed differentiation of functional corticospinal-like neurons from endogenous SOX6+/NG2+ cortical progenitors

Abdulkadir Ozkan*[,a], Hari K. Padmanabhan*[,a], Seth L. Shipman[a,b], Eiman Azim[a,c], Priyanka Kumar[a], Cameron Sadegh[a,d], A. Nazli Basak[e], Jeffrey D. Macklis[a,#]

[a] Department of Stem Cell and Regenerative Biology, and Center for Brain Science, Harvard University, Cambridge, MA, 02138, USA
[b] Current address: Gladstone Institute of Data Science and Biotechnology, San Francisco, CA, 94158, USA
[c] Current address: Molecular Neurobiology Laboratory, Salk Institute for Biological Studies, La Jolla, CA, 92037, USA
[d] Current address: Institute for Pediatric Regenerative Medicine, Shriners Hospitals for Children, Northern California, University of California-Davis, Sacramento, CA, 95817, USA
[e] Koc University, Translational Medicine Research Center, KUTTAM-NDAL, Istanbul, 34450, Turkey
* These authors contributed equally.
[#] Correspondence should be addressed to J.D.M. (jeffrey_macklis@harvard.edu)

Corticospinal neurons (CSN) centrally degenerate in amyotrophic lateral sclerosis (ALS), along with spinal motor neurons, and loss of voluntary motor function in spinal cord injury (SCI) results from damage to CSN axons. For functional regeneration of specifically affected neuronal circuitry *in vivo*, or for optimally informative disease modeling and/or therapeutic screening *in vitro*, it is important to reproduce the type or subtype of neurons involved. No such appropriate *in vitro* models exist with which to investigate CSN selective vulnerability and degeneration in ALS, or to investigate routes to regeneration of CSN circuitry for ALS or SCI, critically limiting the relevance of much research. Here, we identify that the HMG-domain transcription factor *Sox6* is expressed by a subset of NG2+ endogenous cortical progenitors in postnatal and adult cortex, and that *Sox6* suppresses a latent neurogenic program by repressing inappropriate proneural *Neurog2* expression by progenitors. We FACS-purify these genetically accessible progenitors from postnatal mouse cortex and establish a pure culture system to investigate their potential for directed differentiation into CSN. We then employ a multi-component construct with complementary and differentiation-sharpening transcriptional controls (activating *Neurog2*, *Fezf2*, while antagonizing *Olig2* with *VP16:Olig2*). We generate corticospinal-like neurons from SOX6+/NG2+ cortical progenitors, and find that these neurons differentiate with remarkable fidelity compared with corticospinal neurons *in vivo.* They possess appropriate morphological, molecular, transcriptomic, and electrophysiological characteristics, without characteristics of the alternate intracortical or other neuronal subtypes. We identify that these critical specifics of differentiation are not reproduced by commonly employed *Neurog2*-driven differentiation. Neurons induced by *Neurog2* instead exhibit aberrant multi-axon morphology and express molecular hallmarks of alternate cortical projection subtypes, often in mixed form. Together, this developmentally-based directed differentiation from genetically accessible cortical progenitors sets a precedent and foundation for *in vitro* mechanistic and therapeutic disease modeling, and toward regenerative neuronal repopulation and circuit repair.

Introduction

Whether toward functional regeneration of specifically affected neuronal circuitry in disorders of the central nervous system *in vivo*, or for appropriate disease modeling and/or therapeutic screening *in vitro*, reliable approaches to accurately differentiate specific types of affected and relevant neurons are required. Overly broad classes of generic or only regionally similar neurons do not adequately reflect the selective vulnerability of neuronal subtypes in most human neurodegenerative or acquired disorders. Molecular and therapeutic findings using broad or only regionally linked classes of neurons not affected in the disorder of interest are frequently not applicable for the neurons centrally involved.

Extraordinarily diverse neurons across the nervous system, in particular within cerebral cortex, display many distinctive features including cellular morphology, laminar and anatomical position, patterns of input and output connectivity, cardinal molecular identifiers, electrophysiology, neurochemical properties, and ultimately their functional roles[1-7]. Diversity exists not only between broad cell types (e.g. excitatory projection neurons vs. inhibitory interneurons; intratelencephalic vs. cortical output ("corticofugal"; projecting away from cortex) neurons; ipsilateral associative vs. commissural), but even within seemingly homogenous populations of neurons. For example, striking and sharp molecular, connectivity, and functional distinctions exist between both spatially separated subsets and interspersed subsets of CSN, with each molecularly distinct neuronal subpopulation programmed to project to distinct segments of the spinal cord, innervate topographically distinct gray matter areas, and synapse onto distinct subsets of interneurons[8-10]. Importantly, these diverse segmentally-specific subsets have selective vulnerability and/or involvement in distinct human disorders[11].

Such selective involvement reflects differences between specific neuronal subtypes in their molecular regulation during development and/or maturity. Specific subtypes of neurons are thus affected in distinct developmental, neurodegenerative, and acquired disorders of the central nervous system (CNS), typically resulting in irreversible functional deficits[12,13]. Particularly relevant to the work presented here, corticospinal neurons (CSN; sometimes termed "upper motor neurons", UMN) centrally degenerate in amyotrophic lateral sclerosis (ALS) and other motor neuron diseases, along with spinal cord "lower motor neurons", of entirely different developmental origin and function. Further, loss of voluntary and skilled motor function in spinal cord injury (SCI) results from damage to CSN axons in the corticospinal tract[14,15]. For goals including regeneration of

affected circuitry, and optimally informative cellular model systems *in vitro*, it is critical to reproduce the type or subtype of neurons involved, so insights and/or candidate therapeutic manipulations are valid for the actual neuron types involved pathologically. Notably, no appropriate *in vitro* models exist with which to investigate CSN/UMN selective vulnerability and degeneration in ALS, critically limiting the relevance of much research. In contrast, the availability of useful *in vitro* models of at least immature spinal motor neurons has enabled substantial success in the spinal muscular atrophy (SMA) field, with both modeling and therapeutics (for more detailed discussion, see[16]).

Importantly and in parallel to *in vitro* modeling, one potential regenerative approach for neurodegenerative or acquired disorders is to restore elements of the affected circuitry with new neurons that are engineered to re-establish circuit-appropriate input and output connectivity[17-19]. Previous studies have demonstrated that active and quiescent progenitors exist in restricted regions of the adult brain[20-23], and that new neurons can integrate into preexisting neural circuitry, supporting the feasibility of cellular repair in the CNS[18,24-29]. Although transplantation of *in vitro* generated neurons, either from pluripotent stem cells (PSC) or from other developmentally distant cell types, is one potential approach[30], either *ex vivo* directed differentiation or *in situ* generation of type- or subtype-specific neurons from optimally appropriate, regionally specified resident progenitors offer several advantages. First, either approach is potentially more likely to recapitulate appropriate neuronal identity than pluripotent stem cell approaches, since presumptive partially fate-restricted resident progenitors and the desired neurons share common developmental lineage, originate from the same neural progenitor domains, and were exposed to the same diffusible and local signaling during embryonic development, thus are likely to share significant epigenomic and transcriptomic commonality[31-33]. Avoiding transplantation via *in situ* neurogenesis would offer the additional advantage of circumventing the requirement for new neurons to migrate long distances to their sites of ultimate incorporation from an injection site with favorable local growth conditions, potentially enabling desired integration of newly recruited neurons at the single-cell level[19,30,34], emulating endogenous adult neurogenesis[35-37]; and avoiding pathological heterotopias.

Substantial progress has been made in efforts to reprogram reactive glia *in vitro* and *in vivo* to acquire some form of neuronal identity[38-45]. However, functional repair of specific circuitry requires highly directed differentiation of specific neuronal subtypes (beyond a generic neurotransmitter identity, e.g.), so new neurons can form circuit-appropriate input and output connectivity[46]. Work from our lab and others have advanced this goal by identifying central molecular programs that first broadly, then increasingly precisely, control and regulate specification, diversity, and connectivity of specific cortical projection neuron subtypes during the period of their differentiation[2,7-9,47-59]. According to an emerging model, complementary and exclusionary sets of proneural and class-, type-, and subtype-specific transcriptional controls act in a subtype-, stage-, and dose-dependent manner to direct distinct projection neuron differentiation trajectories, while repressing alternative fates[49]. This sharpens subtype identities and distinctions.

In the work reported here, we build on prior work from our lab[60] identifying *Sox6* as a unique stage-specific, combined temporal and spatial, control over all cortical projection neuron development that is both expressed by all cortical-pallial/excitatory projection neuron progenitors and excluded from subpallial/interneuron progenitors, and that effectively represses the transcriptional expression of the proneural gene neurogenin 2 (*Neurog2*). We identify that a subset of NG2+ endogenous cortical progenitors continue to express *Sox6*, which continues to repress inappropriate *Neurog2* expression and neuronal differentiation. We take advantage of genetic access to FACS-purify these endogenous cortical progenitors and establish a pure culture system to investigate the potential for their directed differentiation into cortical output neurons, the type of clinically relevant neurons that centrally includes CSN.

We then synthesized and applied a multi-component gene expression construct with complementary and differentiation-sharpening transcriptional controls (activating *Neurog2* and *Fezf2*, while antagonizing *Olig2* with *VP16:Olig2*) to these purified, partially fate-restricted progenitors from postnatal mouse cortex. We find that this approach directs highly specific acquisition of many cardinal morphological, molecular, and functional characteristics of endogenous corticospinal neurons, and not of the alternative intracortical or other CNS neuronal subtypes. We further investigate these results in several directions, finding, e.g., that *Neurog2* alone is not sufficient to induce a specific neuronal identity; that neurons induced by *Neurog2* instead exhibit aberrant multi-axon morphology, and express molecular hallmarks of alternate cortical projection subtypes, often in mixed form.

As a proof-of-concept, we employ synthetically modified RNAs to control timing and dosage of the exogenous transcription factors, finding that a single pulse of *Neurog2* combined with *Fezf2* induces projection neuron differentiation from cultured SOX6+/NG2+ endogenous cortical progenitors, further highlighting the seemingly "poised" and already partially cortical neuron fate-directed potential of these specialized progenitors. Our results demonstrate the feasibility of achieving molecularly directed, subtype-specific neuronal differentiation from a widely distributed endogenous progenitor population, with significant implications for both *in vitro* disease modeling and efforts toward therapeutic *in situ* repopulation of degenerated or injured cortical circuitry.

Results

Identification of SOX6+/NG2+ cortical progenitors in postnatal and adult neocortex

Progenitors and glia in postnatal and adult cortex share a common ancestry with cortical neurons[61]; they are exposed to the same morphogen gradients throughout embryonic development, and, thus, compared to distant cell types, have similar epigenomic and transcriptomic landscapes[62,63]. Therefore, we hypothesized that at least some of these

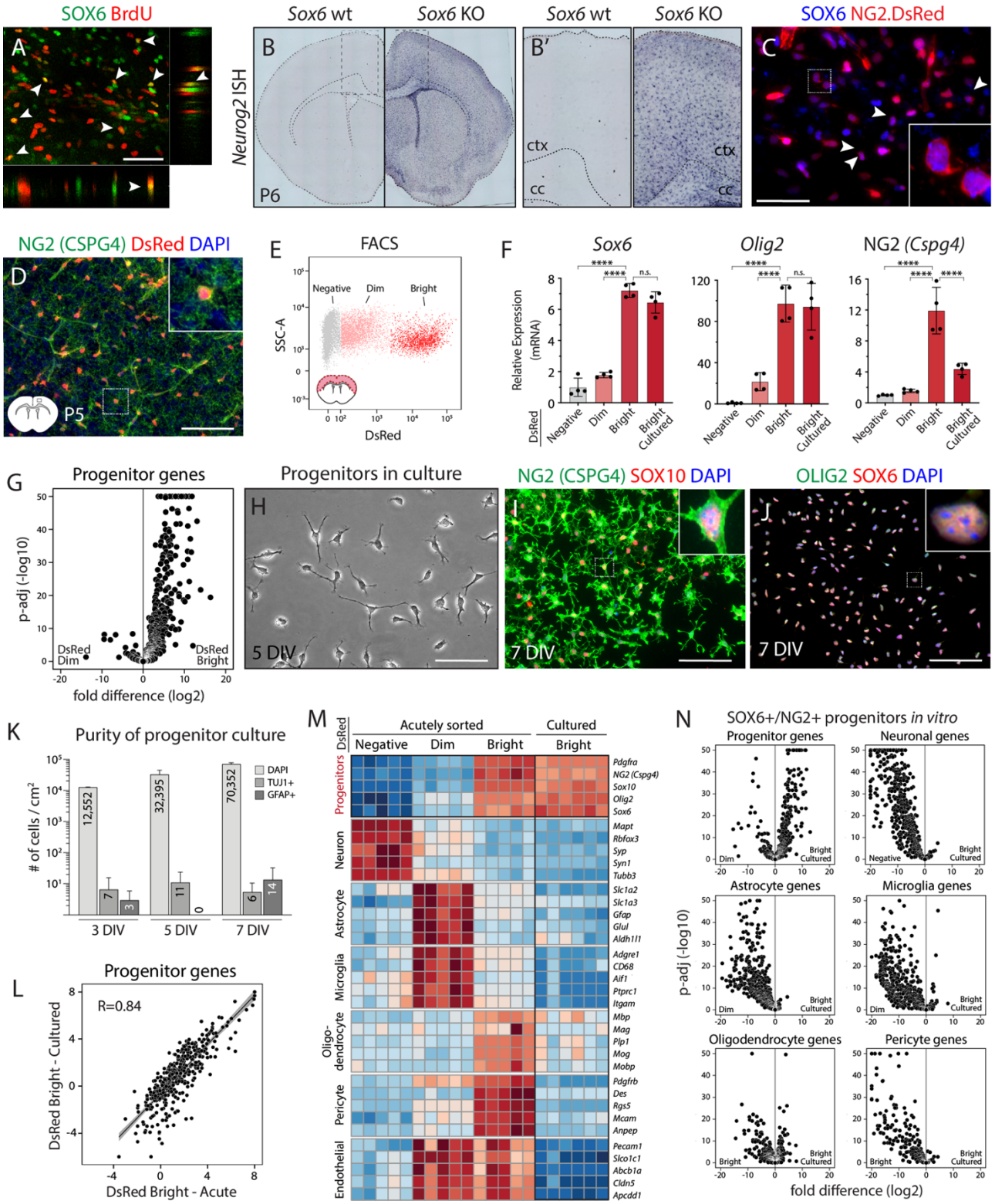

progenitors and glia might have dormant neurogenic potential, and that a subset might have molecular characteristics that might enable their enhanced and potentially appropriate differentiation into cortical projection neurons.

To identify this potential subset, we labeled proliferative cells in postnatal and adult cortex with an injection of BrdU (see Methods), and immunolabeled for PAX6, TBR2, SOX6, and FEZF2 -transcriptional controls that play key roles in embryonic pallial progenitors[2,64,65]. This experiment revealed that many BrdU+ proliferative cells continue to express SOX6 in postnatal and adult mouse cortex (Figures 1A and S1). *Sox6* controls molecular segregation of dorsal and ventral telencephalic progenitors during telencephalon parcellation in important part by blocking ectopic proneural gene expression by pallial progenitors and

subpallial mantle zones[60]. To investigate whether *Sox6* has parallel function in postnatal proliferative cells, we investigated proneural gene expression in *Sox6* null brains. Strikingly, the proneural gene *Neurog2* is ectopically expressed throughout *Sox6*-null cortex at postnatal day 6 (P6) (Figure 1B). This result indicates that a subset of postnatal cortical progenitors maintains latent neurogenic programs that are actively suppressed by *Sox6*, similar to its function in embryonic progenitors.

We then focused investigation on SOX6+ cells by immunocytochemistry (ICC), and identify that they are a subset of NG2-proteoglycan-expressing proliferative cells resident across the CNS (Figure 1C). These data indicate that at least a subset of SOX6+/NG2+ progenitors resident in the neocortex possess some level of dormant neurogenic competence, which might be activated with relatively focused molecular manipulation. Therefore, we targeted SOX6+/NG2+ progenitors for directed differentiation into clinically relevant cortical output neurons, including CSN.

Purification and culture of SOX6+/NG2+ cortical progenitors

We established a culture system of purified SOX6+/NG2+ cortical progenitors to evaluate candidate transcriptional regulators for their ability to direct differentiation of SOX6+/NG2+ progenitors into cortical output neurons *in vitro*, thus enabling rigorous and iterative experimentation under controlled conditions. We used a transgenic NG2-DsRed mouse line (Figures 1D and S2A-S2C)[66] to isolate DsRed-positive cells by FACS from micro-dissected dorso-lateral neocortex at P2-P6 (Figure 1E). Two distinct populations of DsRed-positive cells were identified based on fluorescence intensity: "DsRed-Bright" (2-5% of total) and "DsRed-Dim" (>20% of total) (Figure 1E). Quantitative PCR (qPCR) (n=4) and ICC (n=2) revealed that DsRed-Bright cells are progenitors with high expression of *Sox6*, *NG2*, and *Olig2* (Figures 1F and S2D), whereas DsRed-Dim cells are a heterogeneous population that includes GFAP+ astrocytes, NESTIN+ progenitors, and a subset of NG2+ progenitors (Figures S2E-S2G). To further investigate these DsRed+ populations, we performed RNA-seq on acutely sorted DsRed-Bright, DsRed-Dim, and DsRed-negative populations (n=5-6), and evaluated expression of a focused set of 500 genes most enriched in major cortical cell lineages (Supplementary Table S1)[63]. Cortical NG2+ progenitor-enriched genes are highly expressed by the DsRed-Bright population (Figures 1G and S3A), whereas neuronal, astroglial, and microglial genes are depleted (Figures S3B-S3D). Together, these data indicate that DsRed-Bright cells are canonical SOX6+/NG2+ progenitors, potentially optimally suited for use in subsequent directed differentiation experiments.

We FACS-purified DsRed-Bright SOX6+/NG2+ progenitors with stringent gating, and cultured them for 5 days (days-in-vitro, DIV) until they reached optimal confluency for transfection (Figure 1H). To promote preservation of endogenous progenitor characteristics in culture, we optimized serum-free medium formulation based on previously published protocols (Figure S2H)[67]. When cultured in this medium, progenitors proliferate robustly in response to the mitogens PDGF-A and FGF2 (Figures S2I-S2N). They maintain their cardinal molecular hallmarks, including expression of SOX6, NG2, OLIG2, and SOX10 (Figures 1F, 1I, 1J, and S2J-S2M), and conserve characteristic branched morphology with non-overlapping territorial processes (Figures S2N-S2P)[68].

We next investigated the extent of spontaneous oligodendrocyte differentiation from these progenitors in culture, since a substantial subset of broad NG2+ progenitors produces oligodendrocytes *in vivo*[66]. Previous work demonstrated that *Sox6* is expressed by at least some proliferating NG2+ progenitors, and is down-regulated upon differentiation[69,70]. Under our culture conditions, FACS-purified cortical SOX6+/NG2+ progenitors continue to express *Sox6* (Figures 1F and 1J), indicating maintenance of their progenitor state. ICC for O4

Figure 1. Identification and culture of SOX6+/NG2+ cortical progenitors with high purity and fidelity

(A) Confocal micrograph of mouse neocortex at postnatal day 7 (P7) showing expression of SOX6 by a subset of BrdU+ proliferative cells. See also Figure S1.

(B) *In situ* hybridization of *Neurog2* in *Sox6* wild-type (wt) (left) and knockout (KO) (right) cortex at P6. (B') Insets showing the boxed areas in B. Loss of *Sox6* results in widespread ectopic expression of *Neurog2* (B').

(C) Immunofluorescence showing expression of SOX6 by DsRed+ NG2+ progenitors in cortex at P5.

(D) Immunostaining of NG2 proteoglycan in NG2-DsRed cortex at P5 shows expression of DsRed by NG2+ progenitors. Inset: a cell with strong DsRed signal in the cell body, and NG2 proteoglycan around the main cell body and in cellular processes. See also Figures S2A-S2C.

(E) Representative FACS plot of neocortical cells from NG2-DsRed transgenic cortex showing distinct DsRed-Bright, -Dim, and -negative populations.

(F) qPCR analysis of *Sox6*, *Olig2*, and *NG2* (a.k.a. *Cspg4*) from acutely sorted DsRed-Negative, -Dim, and -Bright populations, as well as cultured DsRed-Bright cells (5DIV), demonstrates that SOX6+/NG2+ progenitors are enriched in DsRed-Bright population and maintain key gene expression *in vitro*. See also Figures S2D-S2G. Data are presented as mean ± SD, n=4, biological replicates, *Actb* normalized data relative to DsRed-negative population. ****$p < 0.0001$, $p \geq 0.05$, no statistically significant difference (n.s.); ANOVA Tukey's post hoc test.

(G) Volcano plot comparing fold difference in average expression of progenitor genes between acutely sorted DsRed-Bright and -Dim populations (RNA-seq, n=5, biological replicates). See also Figure S3A.

(H) Representative brightfield image of cultured SOX6+/NG2+ (DsRed-Bright) progenitors at 5 DIV showing preserved progenitor multipolar morphology. See also Figures S2J-S2P.

(I and J) Cultured progenitors continue expressing the key progenitor-specific molecules NG2, SOX10 (I), OLIG2, and SOX6 (J) at 7 DIV.

(K) Quantification of TUJ1+ and GFAP+ cells at 3-, 5-, and 7 DIV shows essentially no contaminant cells in culture. Data are presented as mean ± SD, n=2, biological replicates. See also Figure S2Q.

(L) Pearson correlation analysis of progenitor genes shows high similarity between acutely sorted and cultured SOX6+/NG2+ (DsRed-Bright) progenitors ($R = 0.84$, $p < 2.2e-16$). Data points represent log2 fold differences in gene expression relative to acutely sorted DsRed-Dim population. See also Figure S3A.

(M) Heatmap of the top five marker genes for seven major cell types in brain shows that SOX6+/NG2+ progenitors are enriched in DsRed-Bright populations and that progenitor cultures are free of potential contaminants. Counts are variance-stabilizing transformed (vst) normalized data in log2 scale.

(N) Volcano plot comparing fold differences in average expression of the top 500 genes for major cell types between cultured SOX6+/NG2+ (DsRed-Bright) progenitors and acutely sorted cells. n=5/6, biological replicates. See also Figure S3.

Scale bars (A, C, H) 50 µm; (D, I, J) 100 µm. cc: corpus callosum, ctx: cortex.

expression (a marker for pre-myelinating oligodendrocytes) revealed that only ~0.15% of these cells express O4 at 3 and 5 DIV (~51 and ~49 O4+ cells/cm^2, respectively). Similarly, qPCR for myelin basic protein (*Mbp*), a canonical oligodendrocyte marker, demonstrated that *Mbp* expression does not increase when cells cultured for 3 or 5 days, compared to acutely sorted progenitors (n=4) (Figure S2E). Together, these data indicate that our culture conditions are not permissive for oligodendrocyte differentiation, and that the purified SOX6+/NG2+ progenitors maintain their progenitor state.

Next, we applied multiple analyses to identify whether there exist contaminant neurons or astrocytes in these cultures of SOX6+/NG2+ progenitors. To identify non-progenitor cells in culture, we immunolabeled for TUJ1 (antibody against TUBB3, a common immature neuronal marker) and GFAP (expressed by astrocytes and some other types of neural progenitors) at 3, 5, and 7 DIV (Figure 1K). At 3 DIV, among ~12,000 total cells/cm^2, there were 7 TUJ1+ cells and 3 GFAP+ cells. At 5 DIV, among ~32,000 total cells/cm^2, there were 11 TUJ1+ cells and 0 GFAP+ cells. At 7 DIV, among ~70,000 total cells/cm^2, there were 6 TUJ1+ cells and 14 GFAP+ cells (Figure 1K). These data reveal the exceptional purity (>99.9% pure) of these primary cultures of FACS-purified SOX6+/NG2+ cortical progenitors. Reinforcing these immunocytochemical results, qPCR revealed that neither *Tubb3* nor *Gfap* are detected in these cultures at 5 DIV, nor in acutely sorted DsRed-Bright cells (n=4) (Figure S2E). In striking contrast, and reinforcing that these culture conditions maintain progenitor competence of SOX6+/NG2+ progenitors, supplementing medium with serum resulted in downregulation of *Sox6* and *NG2*, and increased expression of *Gfap* (n=4) (Figure S2Q). Together, these results identify that there is essentially no contamination under these culture conditions at any time point investigated, and that progenitors maintain their molecular and functional characteristics *in vitro*.

We further investigated the progenitor cultures for potential pericyte contamination, since pericytes express NG2 proteoglycan[71], so they are DsRed-positive in NG2-DsRed cortex (Figures 1D, S2A, and S2B). qPCR for pericyte markers *Pdgfrb* and *Mcam (CD146)* revealed that pericytes are abundant in acutely sorted DsRed-Bright cultures, but are absent in culture at 5 DIV (n=4) (Figure S3F), indicating that pericytes do not survive in these culture conditions. Validating these results by ICC, there were no PDGFRB+ cells in culture at either 3 or 5 DIV (0 cells/cm^2, n=2), unless DsRed-Bright cells were cultured in serum-supplemented media (Figures S3J-SL). Together, these results reveal that these culture conditions do not support pericyte survival, and that progenitor cultures are pericyte-free.

To even further investigate by independent means whether progenitors maintain their *in vivo* molecular features *in vitro*, we performed RNA-seq on these cultures at 5 DIV (n=6), evaluating expression of 500 genes most enriched in the major alternative cell lineages (Supplementary Table S1)[63]. The purified SOX6+/NG2+ progenitor cultures express progenitor-enriched genes (Figure 1L), but, appropriately, do not express neuronal-, astroglial-, microglial-, pericyte-, or vascular-enriched genes (Figures 1M, 1N, S3A-S3D, and S3G-S3I), confirming the ICC and qPCR results. Similarly, oligodendrocyte-enriched genes are not upregulated in culture compared to acutely sorted cells (Figures 1M, 1N, and S3E). Importantly, gene expression profiles of cultured progenitors were highly consistent and reproducible across biological replicates (n=6) (Figures S3A-I). Together, these data further confirm that cortical SOX6+/NG2+ progenitors maintain their molecular characteristics *in vitro*, enabling establishment of a robust *in vitro* culture system in which to reproducibly manipulate progenitors under controlled conditions.

Multi-gene construct "NVOF" induces neuronal differentiation and unipolar pyramidal morphology from SOX6+/NG2+ cortical progenitors

To direct differentiation of corticospinal neurons from cortical SOX6+/NG2+ progenitors, we designed a tandem construct containing three transcriptional controls (***N**eurog2*, ***VP16:O**lig2*, and ***F**ezf2*– collectively termed "**NVOF**") based on their developmental functions (Figure 2A and 2B)[72]. The expression of the polycistronic construct is driven by the CMV-β-actin (CAG) promoter, with the open reading frames separated by 2A linker sequences[72], also including a GFP reporter to identify transfected cells.

First, to drive glutamatergic neuronal identity, we selected the pallial proneural transcription factor neurogenin2 (*Neurog2*)[73,74]. Previous data showed that forced expression of *Neurog2* reprograms cultured postnatal glia and human ESC/iPSCs into synapse forming glutamatergic neurons *in vitro*[45,75,76], and can induce immature neuron-like cells from injury induced reactive glial cells in the adult mouse brain[38]. We tested *Neurog2* alone in cultured progenitors and found that, in line with previous reports, *Neurog2* is sufficient to induce neurons with long axons *in vitro* (Figure S4A).

Second, to overcome the predominant gliogenic potential in NG2+ progenitors, we complemented *Neurog2* with *VP16:Olig2* (VP16 transactivation domain from herpes simplex virus fused to an OLIG2 DNA binding domain)[77]. This activator form of *Olig2* functions as a dominant negative to counteract *Olig2* gliogenic function[77-79]. *Olig2*, a bHLH transcription factor, is necessary for the specification of broad population of NG2+ progenitors and for their differentiation into oligodendrocytes[80]. In addition, OLIG2 has been shown to antagonize NEUROG2 activity during neurogenesis to maintain progenitors for subsequent gliogenesis during spinal cord development[81]. Misexpression of *Olig2* in the cortex broadly represses proneural and neurogenic genes, and increases oligodendrocyte precursor cell numbers[82]. Intriguingly, antagonizing OLIG2 function in reactive glial cells after injury results in a substantial number of immature neurons in the cortical or striatal parenchyma[83,84]. To confirm whether *VP16:Olig2* is able to suppress glial differentiation capacity of cortical SOX6+/NG2+ progenitors in our experimental paradigm, we transfected progenitors with either *VP16:Olig2* or control GFP constructs. At 1 DPT, the cultures were treated with thyroid hormone (T3) to induce differentiation of oligodendrocytes. At three-days post-T3 treatment, as expected, control cells differentiated into oligodendrocyte-like cells, whereas

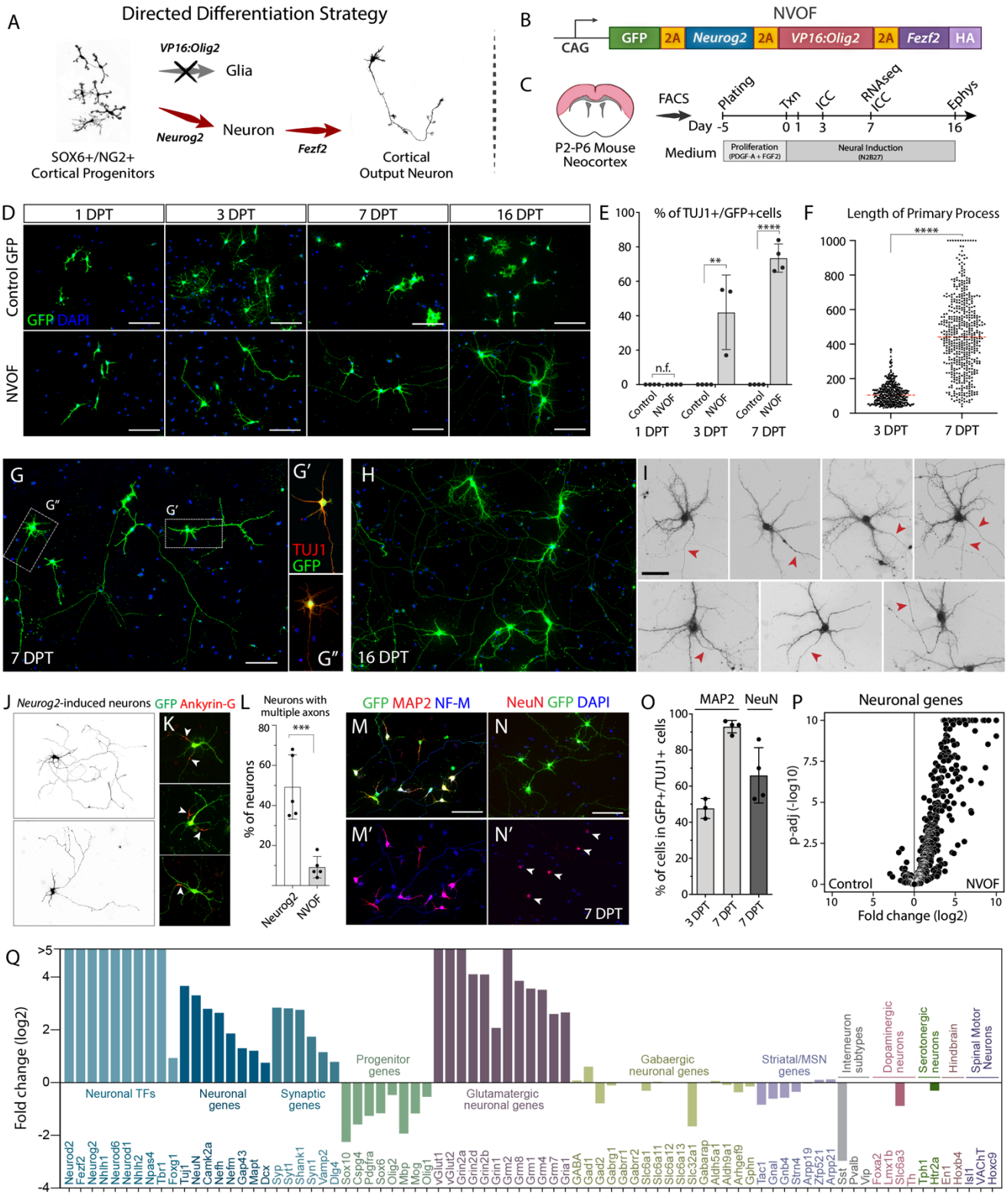

VP16:Olig2 transfected progenitors had remarkably turned into neuroblast-like bipolar cells, indicating that VP16:OLIG2 successfully blocks endogenous OLIG2 function (Figure S4B and S4C).

Third, to induce cortical output neuronal fate, we selected *Fezf2*, an upstream transcriptional regulator that controls specification and development of cortical output neurons during cortical neurogenesis[2,29,47,59] (Figure S4D and S4E, see Discussion). *Fezf2* is capable via single gene over-expression of generating cortical output neuronal fate from alternate cortical progenitors[85], from progenitors of striatal neurons *in vivo*[86], and from intracortical projection neurons post-mitotically in the early postnatal brain[87].

We first verified expression of individual proteins from the polycistronic construct (Figures S4H-S4J), then assessed the construct's functionality in embryonic cortical progenitors *in vivo* (n=3) (Figures S4K-S4N). Previous work has shown that mis-expression of *Fezf2* in late-stage embryonic cortical progenitors modifies their fate to cortical output neurons, re-routing the intracortical axonal trajectories of layer II/III neurons to subcortical targets[85]. To investigate whether this FEZF2 function persists in the presence of NEUROG2 and VP16:OLIG2, we electroporated NVOF into embryonic ventricular zone progenitors *in utero* at E15.5, the peak production of upper layer intracortical neurons, and found that forced expression of NVOF induces cortical output identity in electroporated neurons (Figures S4K-S4N). Unlike control GFP-only neurons (Figures S4K and S4L), many NVOF+ axons descend through the internal capsule, to or past the thalamus (Figure S4M), with some extending into the cerebral peduncle (Figure S4N). These data demonstrate that the NVOF construct is expressed by electroporated neurons, and that *Fezf2* continues to specify cortical output identity when co-expressed with *Neurog2* and *VP16:Olig2*.

We transfected NVOF into cultured cortical SOX6+/NG2+ progenitors at 4-5 days after FACS purification, and analyzed their morphology and expression of cardinal ICC markers of cell type identity over two weeks of differentiation (Figure 2C). Progenitors began to lose multipolar morphology within 24 hours (Figure 2D). By 3 days post-transfection (DPT), many extended a single axon-like neurite (Figures 2D and 2F), and expressed the broad neuronal marker TUJ1 (42%, n=3, >200 cells/experiment) (Figures 2E, S5A, and S5B). This morphological transformation was coupled with loss of the progenitor markers NG2 and SOX10 (Figures S5A and S5B). By 7 DPT, ~73% of NVOF-transfected cells expressed TUJ1, acquired neuronal morphology with dendrite-like features, and extended a single prominent axon-like process (n=4, >200 cells/experiment) (Figures 2D-2G, S5C, and S5D). Consistent with pyramidal neuron morphology, the primary axon-like processes of NVOF-directed neurons underwent significant extension between 3 DPT and 7 DPT, often extending further than 500 µm from the soma (>40%, n=3) (Figure 2F). By 16 DPT, the morphology of these putative neurons became more elaborate; the single long axon-like neurite was maintained, their dendrite-like structures became more tufted, and axon-neurite branches of neighboring cells became intercalated (Figures 2H and 2I).

In striking contrast, progenitors transfected with a control GFP-only construct displayed glial morphology throughout the culturing period, and no GFP+/TUJ1+ cells were present at all (n=4, 250-350 cells/experiment) (Figures 2D and 2E). Further, even among non-transfected, GFP-negative cells, only 5 cells/cm^2 out of ~30,000 progenitors/cm^2 were TUJ1+, and these GFP-/TUJ1+ cells did not increase over time (n=4). These results further reinforce the absence of contaminating progenitors with spontaneous neurogenic characteristics in these cultures, and the lack of spontaneous differentiation by cultured cortical SOX6+/NG2+ progenitors.

Neurog2 is widely used to induce generic excitatory neurons from somatic and pluripotent stem cells[45,75]. We directly compared *Neurog2*-induced and NVOF-induced neurons to determine whether *Neurog2* might be sufficient for induction of equivalent neuronal differentiation from cultured SOX6+/NG2+ cortical progenitors. We transfected cultured progenitors with either *Neurog2*-GFP or NVOF, and analyzed cells at 7 DPT. Though superficially similar in some respects to NVOF-induced neurons (Figure S2J), *Neurog2* induces multipolar neuronal morphology with many dendrite-like structures and multiple long axon-like processes. While almost all NVOF-induced neurons extend a single primary axon (90%), ~50% of *Neurog2*-induced neurons aberrantly extend multiple axon-like ANKYRIN-G+ processes originating from their cell bodies (Figures 2J-2L) (n=5, >100 cells/n). This aberrant, over-exuberant neuritogenesis by *Neurog2*-induced neurons indicates defective polarization, potentially due to a lack of negative feedback signaling for inhibition of surplus axon formation[88].

Figure 2. NVOF induces mature glutamatergic neurons from SOX6+/NG2+ cortical progenitors *in vitro*

(A-C) Strategy for directed differentiation of SOX6+/NG2+ progenitors into cortical output neurons (A), the NVOF multigene construct (B), and the experimental outline (C).
(D) Representative images of control- and NVOF-transfected cells at 1-, 3-, 7-, and 16-days-post-transfection (DPT). Unlike control-transfected cells, NVOF-transfected cells lose progenitor morphology at 1 DPT, and progressively exhibit complex neuronal morphology, including a primary axon-like process and multiple dendrite-like processes.
(E) Percentage of control-GFP and NVOF-transfected cells with neuronal morphology and TUJ1 expression (~42% at 3 DPT and ~74% at 7 DPT for NVOF, n=4, >200 cells/n).
(F) Quantification of primary process length for NVOF-induced neurons at 3- and 7 DPT (n=3, >100 cells/n).
(G) Representative morphology of NVOF-induced, TUJ1+ neurons at 7 DPT. Note the single axon, dendrite-like structures, and multiple axonal collaterals.
(H) Representative images of NVOF-induced neurons at 16 DPT showing acquisition of elaborate dendritic morphology and highly intercalated axonal processes.
(I) High-power representative images of individual NVOF-induced neurons at 16 DPT showing dendritic complexity and a single primary axon-like process for each neuron (red arrows).
(J) Representative images of *Neurog2*-induced neurons with multiple atypical axon-like processes. (GFP is pseudocolored for enhanced clarity of cell morphology.)
(K) Representative images of *Neurog2*-induced neurons expressing the axonal marker ANKYRIN-G (ANK3) by multiple neurites.
(L) Quantification of neurons with single versus multiple axons in *Neurog2*- and NVOF-induced neurons. At 7 DPT, 49% ±16% of *Neurog2*-induced neurons have multiple, long axon-like processes, whereas a small number of such neurons exist after NVOF induction (9% ±5%) (n=5, >100 cell). See methods for details.
(M-N) Representative images of NVOF-induced neurons at 7 DPT showing compartmentalized expression of the somato-dendritic marker MAP2, the somato-axonal marker Neurofilament-M, and the mature neuronal marker, NeuN.
(O) Quantification of NVOF-induced, TUJ1+ neurons expressing MAP2 at 3 DPT (~48%, n=3, >200 cells) and 7 DPT (~93%, n=4, >200 cells), as well as NeuN at 7 DPT (66% ±16%, n=4, >100 cells).
(P) Volcano plot showing upregulation of neuronal genes in NVOF-induced neurons compared to control-transfected cells at 7 DPT (RNA-seq, n=3, biological replicates).
(Q) Bar graph of RNA-seq data displaying upregulation of neuronal genes and downregulation of progenitor genes in NVOF-induced neurons at 7 DPT. Neurons exclusively upregulate glutamatergic genes, but not genes specific to alternate neuronal identities.
Scale bars (D, G, H, J, M, N) 100 µm; (I) 50 µm. Error bars show standard deviations. ****$p < 0.0001$, ***$p < 0.001$, **$p < 0.01$, t-test in (E, F, L). n.f. (no TUJ1+ cell found).

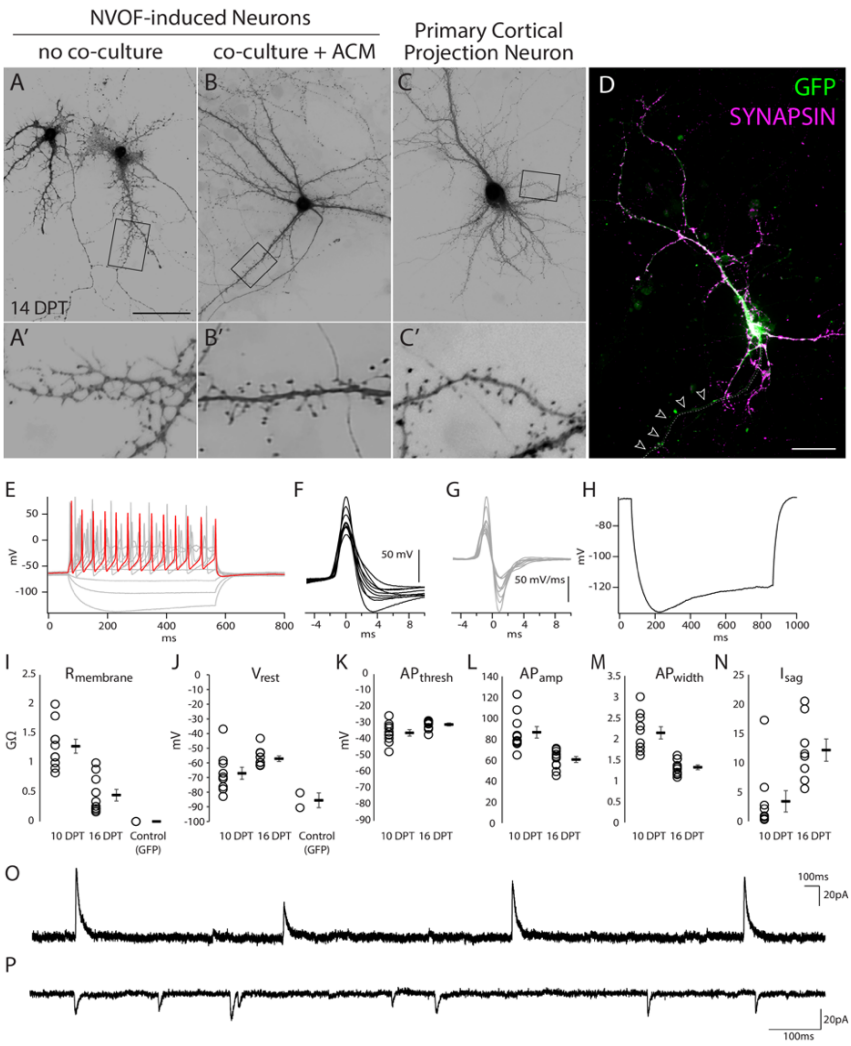

Figure 3. NVOF-induced neurons are electrically active, and have spontaneous synaptic currents

(A-B) Representative high-magnification images of NVOF-induced neurons at 14 DPT (pseudo-colored GFP) with and without co-culture of forebrain primary neurons and astrocyte-conditioned media. (A'-B') Insets showing the boxed areas. Note differences in morphology of presumptive synaptic structures between the two conditions. See methods for details.

(C) Representative high-magnification image of a primary cortical neuron at 14 DPT (pseudo-colored tdTomato) from *in utero* electroporated wild-type mice as a positive control. (C') Note similarity in morphology of presumptive synaptic structures between primary neurons and NVOF-induced neurons in B'. See methods for details.

(D) Representative high-magnification image of a SYNAPSIN-positive NVOF-induced neuron co-cultured with forebrain neurons, indicating abundant connections from surrounding neurons. Arrows show the presumptive single primary axon with no synapsin staining.

(E) A representative NVOF-induced neuron at 10 DPT showing depolarizing steps evoking a train of action potentials (red highlighted trace: step 6, 50 pA). 10 minutes after break-in, or following a resting Vm stabilization greater than 1 minute, cells were injected with 10 current steps ranging from -40 pA to 95 pA in 15 pA increments, for a duration of 500 ms each.

(F) The first evoked action potential in response to positive current injections for 10 individual cells, overlaid (10 DPT). Waveforms are aligned at threshold for comparison.

(G) Corresponding dV/dt traces for action potentials shown in F.

(H) Representative sag current, indicating presence of Ih, induced with a 500 ms current injection of -40 pA (average of 10 sweeps).

(I) Cell membrane resistance decreases over time (10 DPT, n=10; 16 DPT, n=10), and is substantially lower without NVOF (GFP, n=2).

(J) Resting membrane voltage for each condition (10 DPT, n=10; 16 DPT, n=10; GFP, n=2).

(K-M) Action potential threshold, amplitude, and width at 10 DPT (n=10) and 16 DPT (n=10).

(N) Sag current at 10 DPT (n=9) and 16 DPT (n=8).

(O) Representative spontaneous outward synaptic currents recorded at -70mV in NVOF+ cells at 16 DPT.

(P) Representative spontaneous inward synaptic currents recorded at -70mV in NVOF-induced neurons at 16 DPT.

Scale bars (A-D) 50 μm; (F) 50 mV; (G) 50 mV/ms. For all graphs I-N, open circles are individual cells, filled boxes are mean ± s.e.m.

NVOF-induced neurons exhibit cardinal features of mature functional neurons

We investigated further whether NVOF-induced, TUJ1+ cells acquire the cardinal molecular hallmarks of mature neurons. At 7 DPT, NVOF-induced neurons express the somato-dendritic marker MAP2 (>90%, n=4, 130-200 cells/n) and the somato-axonal marker NF-M (Figures 2M and 2O), indicating clear polarization and dendritic compartmentalization. Dendrite formation was confirmed by high-power imaging at 16 DPT, revealing that the NVOF-induced neurons have dendrite-like processes with filopodial protrusions, and a single axon-like primary process lacking dendrite-like structures (Figure 2I, highlighted with red arrows). Further, at 7 DPT, NVOF-induced neurons express neuronal nuclear antigen (NeuN) (66 ± 16%, n=4, >100 cells/n) (Figures 2N and 2O), polysialylated neural cell adhesion molecule (PSA-NCAM or *Ncam1*) (Figures S5F and S5G), the presynaptic molecule synapsin (Figure S5H), with some displaying synaptophysin in axonal branches and tips of axonal protrusions (Figure S5I), and *vGlut1* (vesicular glutamate transporter 1) (Figure S5J), indicating glutamatergic identity. Together, these data indicate that NVOF robustly induces neuronal differentiation and maturation by cortical SOX6+/NG2+ progenitors *in vitro*.

To determine whether neuronal differentiation from these cortical SOX6+/NG2+ progenitors requires an intermediate proliferative step, we pulsed cultures with BrdU for 15 hours after transfection, and labeled GFP+ cells (NVOF-transfected or GFP-only controls) for BrdU by ICC at 3 DPT (n=2). Some previous work has reported that cell division is not required for neuronal differentiation from resident glia[45]. While a majority of cells transfected with GFP-only were BrdU+, only rare NVOF-transfected cells were BrdU+. This result indicates that NVOF causes rapid cell cycle exit, and that chromatin reorganization during cell division is not required for NVOF-induced neuronal differentiation and maturation from SOX6+/NG2+ progenitors.

To more broadly investigate the molecular identity and specificity of neurons induced from cortical SOX6+/NG2+ progenitors transfected with NVOF, we performed RNA-seq on control GFP-transfected and NVOF-transfected cells at 7 DPT (n=3) (Figures S6A and S6B). NVOF-induced neurons have decreased expression of progenitor genes, and increased expression of neuronal genes, relative to GFP-transfected cells

(Figures 2M and S6C). Upregulated neuronal genes include proneural transcription factors, neuron-specific cytoskeletal molecules, and molecules that function in synaptic transmission, dendritic specialization, glutamatergic signaling, axon guidance, and neuronal connectivity (Figures 2P, 2Q, and S6D). *Neurog2* is required for the differentiation of multiple neuronal types across regions of the nervous system and overexpression of *Neurog2* in somatic and stem cells generates neurons with mixed identities[76,89-93]. We therefore confirmed that NVOF-induced neurons express exclusively genes typical of glutamatergic neurons, but not genes specific for alternate neuronal types (e.g. GABAergic interneurons, striatal projection neurons, or serotonergic, dopaminergic, hindbrain, or spinal motor neurons) (Figures 2Q and S6E-S6N).

We co-cultured NVOF-transfected cells at 1 DPT with primary forebrain cells from mouse cortex in astrocyte-conditioned media (Figure S5K) (see Methods) to investigate whether such a potentially permissive and/or instructive environment might even further enhance neuronal differentiation and maturation. It is known that neurons cultured below critical density, or in the absence of glial-derived trophic factors, often survive poorly and/or do not mature[94,95]. Indeed, culture with primary neurons increased morphological maturation of NVOF-induced neurons, resulting in elaborate dendrites with abundant synapses (n=2) (Figures 3A-3D and S5L-S5N), demonstrating synaptic input from surrounding neurons, and functional integration into neuronal networks. Quite notably, the morphology and density of dendritic synapse-like structures in NVOF-induced neurons were essentially indistinguishable from those of primary cortical neurons cultured under identical conditions (Figures 3A-3D).

To investigate functional properties of NVOF-induced neurons, we performed whole-cell patch-clamp recordings at 10 DPT (without co-culture) and at 16 DPT (with primary neuron co-culture) (Figures 3E-3P). Consistent with their immunocytochemical and morphological characteristics, NVOF-induced neurons possess electrophysiological hallmarks of neurons, including trains of action potentials upon depolarizing steps (Figures 3E-3G), HCN-channel currents (Isag) upon hyperpolarization (Figure 3H), and spontaneous synaptic currents (Figures 3O-3P). NVOF-induced neurons also mature over time in culture, with overall increases in the action potential threshold (-35.9 mV at 10 DPT versus -30.9 mV at 16 DPT) (Figure 3K), decreases in action potential width (2.1 ms at 10 DPT versus 1.3 ms at 16 DPT) (Figure 3M), and increases in Isag (3.4 mV at 10 DPT versus 12.1 mV at 16 DPT) (Figure 3N). Cortical SOX6+/NG2+ progenitors transfected with the control vector possess membrane resistances and resting voltages that are inconsistent with neuronal identity (Figures 3I and 3J).

Vector-free induction of neuronal differentiation from cortical SOX6+/NG2+ progenitors with synthetic modified mRNAs

The results presented above reveal that NVOF-induced neurons express a quite comprehensive set of molecules that indicate faithful neuronal differentiation, and that they possess electrophysiological properties indistinguishable from those of primary neurons. However, previous work reports that sustained expression of *Neurog2* can be deleterious to differentiating cortical neurons[96]. To more closely reproduce the dynamics of developmental expression of *Neurog2*, we aimed to restrict *Neurog2* expression to a short, early time period using synthetic, chemically-modified RNA in which one or more nucleotides are replaced by modified nucleotides. Previous work, in multiple systems, has revealed that synthetic modified mRNA mediates highly efficient, integration-free, transient protein expression *in vitro* and *in vivo* without eliciting an innate immune response[97,98].

In contrast to the transient expression of *Neurog2* during neurogenesis *in vivo*, cortical output neurons express *Fezf2* throughout development and adulthood[85]. To emulate the distinct kinetics of endogenous developmental expression of *Neurog2* and *Fezf2*, we devised a strategy by which *Neurog2* is transiently expressed via synthetic modified mRNA, and *Fezf2* is expressed on an ongoing basis as a plasmid DNA construct with a constitutively active CAG promoter. We first adapted our transfection protocol to transfect cortical SOX6+/NG2+ progenitors with mRNA at high efficiency (Figures S7A and S7B). To test feasibility of DNA-RNA co-transfection, we co-transfected tdTomato as a plasmid DNA, and GFP as a synthetic modified mRNA (Figure S7C). ~50% of fluorescent cells were co-transfected with both reporters (n=3). We investigated dynamics of protein expression, finding that the GFP synthetic modified mRNA displays peak protein levels 12-24 hours post-transfection, then declines (Figures S7D-S7G).

Next, we directly compared the efficacies of a *Neurog2* DNA construct and a *Neurog2* synthetic modified mRNA. Strikingly, confirming the neurogenic competency of cortical SOX6+/NG2+progenitors, one dose of *Neurog2* synthetic modified mRNA induces robust neurogenesis, albeit with lower efficiency than *Neurog2* DNA or NVOF (n=3) (Figures S7H and S7I). We then co-expressed *Neurog2* in synthetic modified mRNA form and *Fezf2* as a plasmid DNA construct. Remarkably, this combination of synthetic modified mRNA plus plasmid DNA produced abundant neurons morphologically indistinguishable from NVOF-induced neurons (Figure S7J). These results reveal that synthetic modified mRNA transfection can be used to tailor more precise kinetics of developmental genes toward directed differentiation of neuronal subtypes.

NVOF-induced neurons acquire molecular hallmarks of cortical output neuron identity *in vitro*

We progressively focused our investigations to evaluate whether NVOF-induced neurons *in vitro* express cardinal molecular hallmarks of endogenous cortical output neurons, with a particular focus on the major output neuron subgroup of subcerebral projection neurons (SCPN, comprising neuronal subtypes that project to brainstem and spinal cord). Results reveal that ~58% of NVOF-induced neurons at 7 DPT express BCL11b/CTIP2, a transcription factor that regulates outgrowth, guidance, and fasciculation of SCPN/CSN axons[47] (n=6, ave 177 cells/experiment) (Figures 4A, 4G, and 4H), whereas no control GFP-only cells express CTIP2 (n=2, ave 207 cells/experiment). NVOF-induced neurons also express PCP4 (Purkinje cell protein

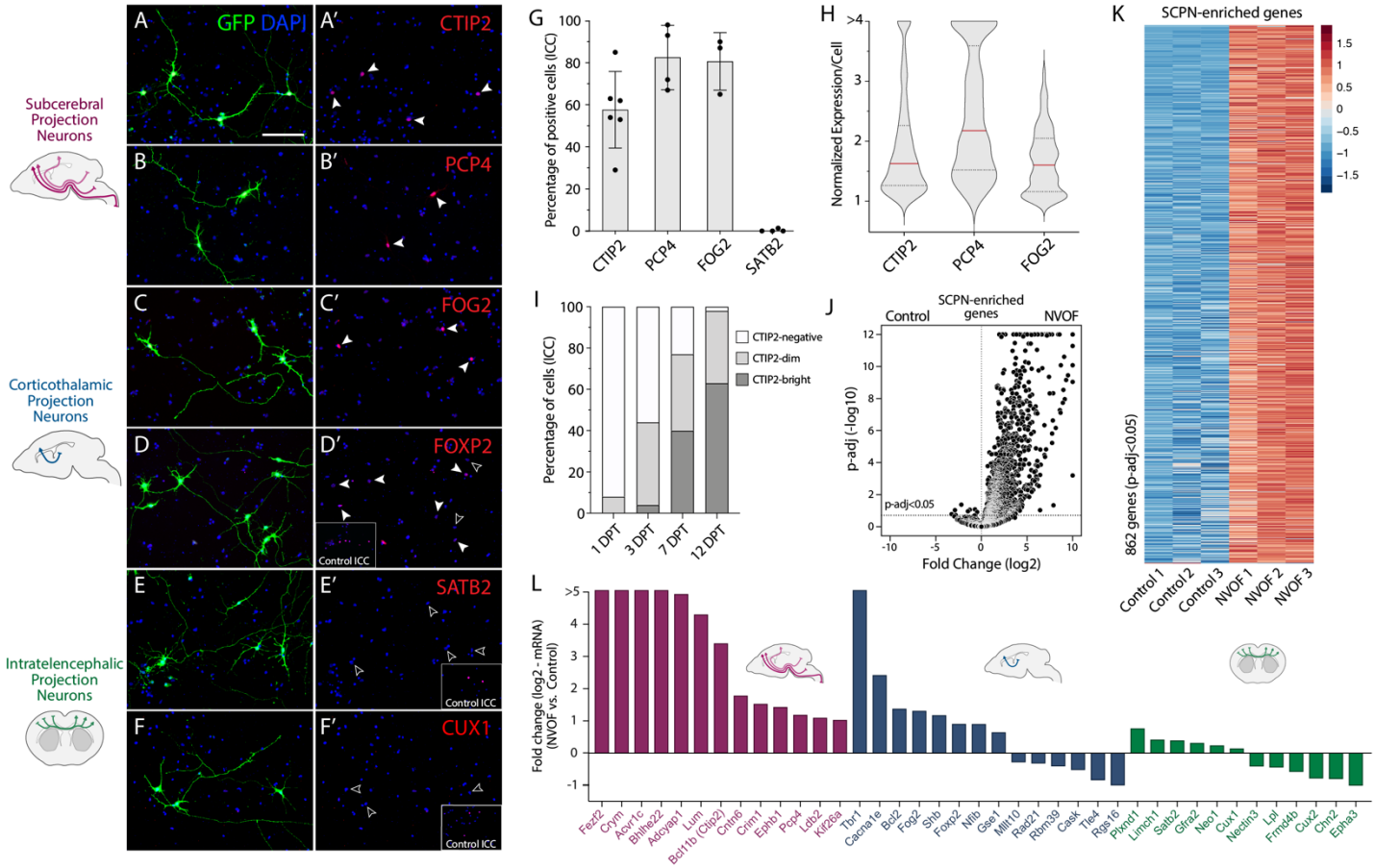

Figure 4. NVOF-induced neurons exhibit molecular hallmarks of corticospinal neurons *in vitro*

(A-F) Representative immunocytochemistry images of NVOF-induced neurons expressing the subcerebral projection neuron (SCPN) transcriptional controls CTIP2 (A) and PCP4 (B), the corticothalamic projection neuron (CThPN) transcriptional controls FOG2 (C) and FOXP2 (D), but not the callosal projection neuron (CPN) molecular controls SATB2 (E) and CUX1 (F). Scale bars (A-F) 100 µm.

(G) Percentage of NVOF-induced, TUJ1+ neurons expressing CTIP2 (56% ±20%, n=5), PCP4 (77% ±14%, n=3), FOG2 (81% ±13%, n=3), and SATB2 (0%, n=3). Error bars show standard deviations.

(H) Violin plot shows mean intensities of CTIP2, PCP4, and FOG2 fluorescence signals in nuclei of NVOF-induced neurons. Plotted values are mean nuclear intensity of individual neurons normalized to the average intensity of the three lowest-expressing neurons. Red line shows median expression, and dark gray lines show quartile expressions.

(I) Bar plot showing percentages of CTIP2-negative, -dim, and -bright neurons at 1-, 3-, 7-, and 12-DPT.

(J-K) Volcano plots and heatmaps of neurons transfected with control GFP and NVOF 7 DPT, displaying the 862 genes enriched in SCPN primary neurons compared to control-transfected cells. See methods for details.

(L) Bar plot of RNA-seq data showing upregulation of SCPN (purple) and CThPN (blue) marker genes, and no activation or downregulation of CPN (green) genes by NVOF-induced neurons relative to neurons transfected with control GFP at 7 DPT.

4), a calmodulin-binding protein reproducibly expressed by SCPN/CSN[47] (~83% at 7 DPT, n=4, ave 131 cells/experiment) (Figures 4B, 4G, and 4H). Importantly, the number of CTIP2+ NVOF-induced neurons continued to increase over time, indicating continued subtype differentiation after 7 DPT (Figure 4I).

Next, we investigated NVOF-induced neurons for expression of corticothalamic projection (CThPN) neuron-enriched molecular controls. Intriguingly, most NVOF-induced neurons express FOG2 (ZFPM2) (~79% at 7 DPT, n=4, ave 132 cells/experiment) (Figures 4C, 4G, and 4H), a critical regulator of CThPN axonal targeting and diversity[58]. However, FOXP2, a transcriptional control required for CThPN specification[99], is expressed heterogeneously by NVOF-induced neurons, with minimal to no expression by many neurons (Figure 4D). These data indicate that NVOF-induced neurons acquire broad cortical output neuronal identity, but refinement of subtype identity (SCPN vs. CThPN) is incomplete, suggesting that additional controls are required for complete subtype refinement.

We also investigated the possibility of subtype "confusion" during directed differentiation by examining whether NVOF-induced neurons also or alternatively express cardinal molecular markers of callosal projection neurons (CPN) or other intra-cortical projection neurons. If identified, this would indicate either immature differentiation or mixed/hybrid identity that is commonly observed with ES/iPSC-derived neurons[100]. Quite notably and appropriately, NVOF-induced neurons do not express SATB2 (0% at 7 DPT, n=4, ~130 cells/n) (Figures 4E and 4G) or CUX1 (n=3) (Figure 4F), molecular controls that are expressed by CPN and other intracortical projection neurons.

Reinforcing and extending these ICC results, RNA-seq reveals that NVOF-induced neurons express many SCPN/CSN-enriched

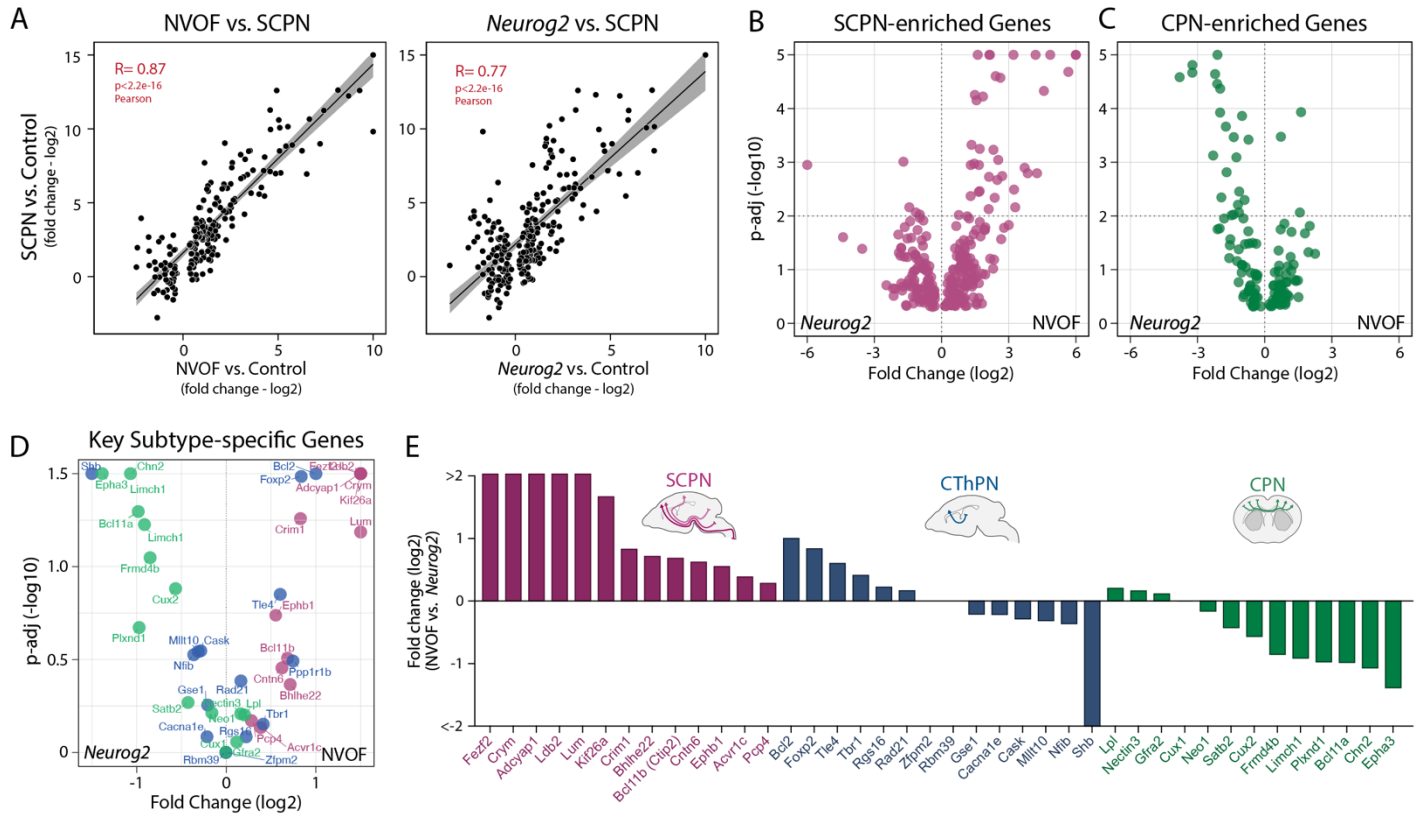

Figure 5. Unlike NVOF-induced neurons, *Neurog2*-induced neurons exhibit unresolved subtype-specific molecular features

(A) Pearson correlation analysis shows high similarity between NVOF-induced neurons at 7 DPT and primary SCPN at P2 (R: 0.87). Compared to NVOF, *Neurog2*-induction (7 DPT) leads to decreased similarity with primary SCPN at P2 (R: 0.77). Data points are log2 fold differences of gene expression at 7 DPT by NVOF- or *Neurog2*-induced neurons (on X-axis) and by SCPN (on Y-axis) compared to progenitors transfected with control GFP.

(B) Volcano plot showing fold differences of SCPN-enriched genes between NVOF- and *Neurog2*-induced neurons.

(C) Volcano plot showing fold differences of CPN-enriched genes between NVOF- and *Neurog2*-induced neurons.

(D-E) Direct comparison of NVOF- versus *Neurog2*-induced neurons at 7 DPT for select developmental genes with key roles in specification and differentiation of SCPN, CPN, and CThPN. Scatter plot (D) and bar graph (E) shows fold differences in gene expression.

genes (Figure 4K) (see methods), including key molecules with central functions in subtype specification of SCPN/CSN (Figure 4L), along with some CThPN-enriched genes (e.g., *Tbr1*, *Fog2*, and *Foxp2*) (Figure 4L). In accordance with the ICC results, RNA-seq reveals that NVOF-induced neurons have no or minimal expression of genes specific to CPN or other intracortical projection neurons, including *Satb2*, *Cux1*, and *Cux2* (Figure 4L). Together, these results indicate that NVOF-induced neurons acquire cortical output neuron identity, primarily of SCPN/CSN, but with some CThPN features, without fully refining molecular identity between these subtypes of cortical output neurons (see discussion).

We directly compared expression of key subtype-specific molecular controls between NVOF-induced and *Neurog2*-induced neurons (Figure S8). While *Neurog2*-induced neurons approximate elements of NVOF induction, with some expression of cortical output neuron markers CTIP2, PCP4, and FOG2 (Figure S8A), and not the CPN and other intracortical neuronal molecules such as SATB2 (Figure S8A) and CUX1 (data not shown), NVOF induction generated more neurons expressing CTIP2, PCP4, and FOG2, with higher average expression (n=>3 for e ach marker) (Figure S8A and S8B), indicating substantially enhanced subtype-specific differentiation by *Fezf2*. Reinforcing the interpretation from aberrant multipolar morphology of *Neurog2*-induced neurons that *Neurog2* alone induces "confused" and unresolved differentiation (Figure 2J-2L), *Neurog2*-induced neurons simultaneously express CTIP1 (BCL11a), a CPN molecular control and antagonist of CTIP2[56,57] (Figures S8A-S8D). During cortical development, CTIP1 is initially expressed broadly by postmitotic neurons, but later, through its cross-repressive interaction with CTIP2, its expression resolves to CPN and CThPN, but not SCPN/CSN, at E17. Continued expression of CTIP1 by *Neurog2*-induced neurons further indicates incomplete and unresolved subtype differentiation.

To comprehensively and directly characterize subtype identities induced by NVOF compared with FACS-purified primary SCPN/CSN or the morphologically and molecularly "hybrid" *Neurog2*-induced neurons, we performed RNA-seq on FACS-purified GFP+ neurons generated by NVOF or *Neurog2* at 7 DPT (n=3), and on FACS-purified SCPN/CSN or CPN from P2 mice (n=3) (Figure 5). Pearson correlation analysis for genes enriched in SCPN compared to CPN reveals that NVOF-induced neurons are substantially more similar to primary SCPN/CSN (R = 0.87) than are *Neurog2*-induced neurons (R = 0.77) (Figure 5A). Even more

strikingly, NVOF induces higher expression of many SCPN/CSN genes relative to *Neurog2* alone (Figure 5B), while *Neurog2* simultaneously and aberrantly activates many typically CPN-specific genes that are expressed at E15 in mouse, the peak period of CPN birth and specification (Figure 5C)[101]. In particular, in line with the prior ICC results, NVOF-induced neurons express SCPN/CSN genes with known key functions in subtype-specific development of SCPN/CSN at higher levels (e.g. *Ctip2* and *Ephb1*, both essential for SCPN/CSN axon guidance) (Figures 5D, 5E)[47,102]. NVOF-induced neurons express *Lumican* and *Crim1*, recently identified to be expressed highly selectively by bulbo-cervical and thoraco-lumbar CSN, respectively, and to regulate their segmentally specific axon targeting[8-10]. In striking contrast, *Neurog2*-induced neurons express many cardinal CPN genes at high levels (e.g. *Epha3* and *Satb2*, which both regulate CPN connectivity)[103,104] (Figures 5D and 5E), further reinforcing that *Neurog2* alone is insufficient for appropriate and resolved differentiation of SOX6+/NG2+ progenitors to cortical output identity.

Together, these results highlight that optimized directed differentiation is achieved by emulating normal developmental steps of sequential subtype specification of neocortical neurons regulated by interactions between broad proneural programs and lineage-specific transcription factors with dynamic temporal expression and cross-regulatory activities.

Discussion

In the work presented here, we first FACS-purify and characterize a relatively rare subpopulation of postnatal cortical progenitors that are molecularly related to early developmental cortical projection neuron-specific progenitors, which express *Sox6*. These postnatal progenitors express both *Sox6* and NG2, and have broad transcriptional profiles of quiescent progenitors. We next identify that developmental transcriptional controls can direct the differentiation of SOX6+/NG2+ cortical progenitors into CSN-like neurons *in vitro*. *Fezf2*, a molecular control over SCPN/CSN development, and transcriptional regulators *Neurog2* and *VP16-Olig2* (together, "NVOF") are able to activate a dormant neurogenic program and overcome the default postnatal gliogenic differentiation program of these cortical progenitors. This directed differentiation generates neurons with a glutamatergic neuronal identity and specific morphologic, molecular, and electrophysiologic features of cortical output neurons resembling corticospinal/subcerebral projection neurons. Our results reveal that NVOF-directed neurons acquire the key molecular features of mature glutamatergic neurons (e.g. expression of NeuN, vGLUT1, CAMK2A, SYN1, SHANK1, ionotropic and metabotropic glutamate receptors), a cortical projection neuron-like morphology with a single long NF-M+ primary axon and a MAP2+ apical dendrite-like process, the expression of molecular controls specific for SCPN/CSN (e.g. BCL11B/CTIP2, CRYM, EPHB1, and PCP4), and, importantly, do not express molecular markers of alternate fates (e.g. SATB2, BCL11A/CTIP1, CUX1, GABA, DARPP32, TH, 5HT, ISL1). We identify that these critical specifics of differentiation are not reproduced by commonly employed *Neurog2*-driven differentiation. Together, our work indicates that directed differentiation via combinatorial and complementary action of central developmental transcriptional controls enables previously inaccessible specificity in generating defined neuronal subtypes for cellular regeneration or disease modeling of degenerated or damaged neuronal circuitry.

In contrast to *Neurog2*-only activation, NVOF-directed neurons acquire multimodal CSN identity

The neurons differentiated by NVOF closely resemble *bona fide* corticospinal neurons. Direct transcriptomic comparison with primary SCPN/CSN reveals that NVOF-directed neurons express a large number of SCPN/CSN-enriched genes (Figures 4J and 4K), with close similarity to SCPN/CSN (R=0.87) (Figure 5A), and their unipolar somatodendritic-axonal morphology also closely resembles that of purified CSN[105]. In contrast to *Neurog2*-induced neurons, NVOF-directed neurons express multiple genes that typically identify CSN specifically. These include the general indicator *Crymu*, as well as *Lumican* and *Crim1*, expressed highly selectively by bulbo-cervical and thoraco-lumbar CSN, respectively, and regulate their segmentally specific axon targeting[8-10]. Quite importantly, NVOF-directed neurons do not display substantial enrichment of key CPN-specific molecular controls (Figure 5C-5E), indicating that they do not acquire "mixed", "confused" identity. This is all in stark contrast to *Neurog2*-only induced neurons, which display aberrant multipolar morphology, mixed transcriptomic signatures, and substantial co-expression of what are normally developmentally exclusionary differentiation regulators and CPN + SCPN molecular signatures.

While *Neurog2* is expressed dynamically in cortical progenitors during generation of major neuronal subtypes[106], *Neurog2* knockout does not show significant perturbations to the expression of molecular hallmarks of these neurons[107,108]. *Neurog2* misexpression by electroporation during the production of superficial layers does not induce characteristic molecular features of deep layer neurons, although a subset of axons of the transfected neurons are re-directed to the ventral telencephalon[108]. Conversely, genetic deletion of *Neurog2* or shRNA knockdown of *Neurog2* from superficial layer intracortical neurons results in variable defects of midline crossing as well as misrouting of callosal axons toward aberrant cortical and subcortical targets[107]. Together these data suggest that *Neurog2* has only a limited lineage-instructive role over specification of cortical output neurons.

Neurog2 is also expressed by progenitors of spinal motor neurons, sensory neurons, and dopaminergic neurons in the mammalian brain, and regulates their specification and differentiation[76]. Therefore, it is conceivable that *Neurog2* expression will induce a subset of its genomic targets depending on the starting cell population, culture conditions, or *in vivo* context. Further, this subset might not be fully faithful to a particular *Neurog2*-dependent *in vivo* neuronal population. In agreement with this hypothesis, recent reports have identified mixed subtype features in neurons generated from ES/iPS cells by *Neurog2* alone[89,93,109]. Several approaches, including pre-

patterning of progenitors, combinatorial expression of a cocktail of transcription factors, temporal control of *Neurog2* expression, induction of signaling pathways with small molecules, and co-culture with astrocytes, have been successfully used to sharpen cell fate specification[89,93,109,110]. Consistent with these results, our NVOF transcriptional regulator combination robustly generates cortical output neuron-like cells compared to *Neurog2* alone.

Intriguingly, even though NVOF-directed neurons acquire both type-specific identity of cortical output neurons, and highly specific indicators of CSN identity, they do not fully resolve the subtype-specific identities of purely subcerebral vs. corticothalamic (CThPN) neurons. They express *Fog2* and *Tbr1*, markers of corticothalamic neurons that are not normally expressed by most mature SCPN/CSN. SCPN and CThPN together comprise cortical output neurons. SCPN and CThPN are located in deep cortical layers V and VI, respectively, and both subtypes send their axons away from cortex via the internal capsule. Not only do these two subtypes share predominant portions of the molecular developmental programs regulating their specification, post-mitotic differentiation, and axon guidance, but approximately 5% are dual SCPN-CThPN that express both high-level *Bcl11b*/*Ctip2* and *Fog2*, and that send dual projections to both thalamus and subcerebral targets[58,59]. These dual-projecting neurons are thought to "share" cortical output information with multiple targets for sensorimotor integration. It is possible that the neurons generated here by NVOF directed differentiation are dual SCPN-CThPN. Recent results identify that the non-DNA-binding transcriptional co-repressor TLE4 forms a complex with transcription factor FEZF2 to epigenetically regulate *Fezf2* expression level, thus the balance between SCPN and CThPN molecular and projection identity at least through the first postnatal week in mouse[2]. This delineation between SCPN and CThPN follows multiple earlier regulatory steps, e.g. the control by the transcription factor SOX5 over sequential generation of CThPN and SCPN by progressively de-repressing *Fezf2* expression. Thus, resolution between SCPN and CThPN subtypes normally occurs progressively through late differentiation *in vivo*.

More broadly, differential expression of key controls in terms of both their levels and timing of expression, in addition to combinatorial co-expression with other key regulators, delineates differentiation of cortical projection neurons into progressively distinct subtypes with distinct targets and functional circuitry[2,49,56-58,111-113]. For example, *Fezf2* and *Ctip2* are expressed more highly by SCPN/CSN relative to CThPN, but both subtypes are severely affected by loss of *Fezf2* function[85,114]. In this normal developmental context, the partially unresolved state of NVOF-directed neurons might represent a mid-developmental stage of subtype identity acquisition, since early during normal development many molecular controls are expressed broadly, and their expression progressively resolves over time to produce more highly subtype-restricted expression in postnatal cortex[115,116]. Consistent with this interpretation, the observed increase of *Ctip2* expression over time by NVOF-directed neurons (Figure 4I) suggests ongoing subtype identity refinement.

An additional factor in the incomplete delineation of NVOF-directed neurons into SCPN/CSN might be the constitutive expression of *Neurog2*. *Neurog2* expression is normally dynamically regulated in neural progenitors[117]. In addition to its well established role in activation of proneural genes, *Neurog2* might activate some neuronal subtype specific genes, such as *Fog2* and *Ctip2*[74,118]. In this context, co-expression of *Fog2* and *Ctip2* by NVOF-directed neurons might be due, at least in part, to constitutive *Neurog2* expression. To begin to overcome this issue, we applied synthetic modified RNA to enable fine-tuning of both level and temporal dynamics of expression of *Neurog2*, and observed robust neuronal induction. The regulation of both level and temporal dynamics of expression during normal development suggests that level- and temporal-controlled expression of *Neurog2* coupled with sustained expression of *Fezf2* (*Fezf2* is expressed constitutively by SCPN/CSN *in vivo*) might enable more refined differentiation of SCPN/CSN from SOX6+/NG2+ progenitors.

Yet another contributing factor to the lack of full SCPN-CThPN delineation of NVOF-directed neurons might be that the basic neuronal induction medium lacks critical extrinsic factors (e.g. diffusible morphogens and growth factors) required for full neuronal maturation and identity refinement. We and others have reported similar but more severe "stalling" of developmental maturation of ES cell-derived cortical-like neurons under standard culture conditions[100]. Supporting this hypothesis, co-culture of NVOF-directed neurons with primary cortical cells (including glia), and in the presence of astrocyte-conditioned medium, improves their survival, and both morphological and electrophysiological maturation (Figure 3).

Taken together, independent regulation over both level and temporal dynamics of individual transcription factor expression, along with culture in optimized induction medium, might likely generate neurons with even further refined identities and distinction between closely related subtypes.

SOX6+/NG2+ progenitors are a subset of cortical "NG2 progenitors" with distinct molecular and functional features

The broad group of cells often collectively characterized by shared expression of NG2 proteoglycan constitute ~2-3% of neural cells in adult rodent cortex, and are the primary proliferative cell group from early postnatal stages through adulthood and in the aged CNS[123,124]. Recent work reveals that this broad group of "NG2 progenitors" is not a homogeneous population; rather, it consists of at least several subpopulations with distinct molecular, cellular, and functional properties[125-135]. While some NG2-expressing progenitors generate oligodendrocytes throughout life, most of them do not differentiate, and remain proliferative in the cortex[68,130]. A subset of these cells generate protoplasmic astrocytes in the ventral forebrain and spinal cord[66,136], and a smaller subset has been reported to generate neurons in the piriform cortex[137,138] and dorsolateral cortex[131].

During development, diverse sets of NG2-expressing progenitors arise from anatomically and molecularly distinct

dorsal and ventral proliferative zones in sequential waves[139,140]. A substantial proportion of the NG2-expressing progenitors in the cortex (~80% in postnatal rodents) share a common lineage with cortical projection neurons in mice[141] and are thus exposed during early- and mid-development to the same morphogen gradients and epigenetic landscaping. This shared origin and molecular history provides a strong developmental basis for understanding mechanistically why these SOX6+/NG2+ cortical progenitors that originate from the dorsal (pallial) cortical proliferative zone are especially competent for directed differentiation into cortical projection neurons, and cortical output neurons in particular.

Of particular note with regard to potential regenerative applications, repopulation of degenerated or injured neurons in particular, SOX6+/NG2+ progenitors, like NG2-expressing progenitors more broadly, are widely distributed in cortex in a tiled manner. Further, progenitors lost due to differentiation or cell death are replenished by cell division and migration of neighboring progenitors[68,142]. Thus, SOX6+/NG2+ progenitors are already positioned local to sites of existing neuron degeneration or other pathology, thus theoretically avoiding the need for long-distance migration and appropriate positioning that would be necessary for transplanted exogeneous progenitors, induced neurons, or spatially restricted adult neuronal progenitors from adult neurogenic regions such as the anterior subventricular zone or hippocampal dentate gyrus. This broad, tiled distribution adds substantially to their potential for cellular repopulation and regenerative approaches.

Cortical SOX6+/NG2+ progenitors are developmentally poised to generate projection neurons

Our finding that loss of *Sox6* de-represses the proneural gene *Neurog2* strongly indicates that *Sox6* continues to function importantly in regulation of proneural genes in cortical progenitors postnatally, and that SOX6+/NG2+ progenitors actively suppress neurogenic potential. Our observation of *Neurog2* de-repression in the absence of *Sox6* function suggests that downregulation of *Sox6* might be considered as an additional or an alternate molecular regulator for future directed differentiation experiments. Reinforcing this interpretation, even transient expression of *Neurog2* alone via a single dose of synthetic modified mRNA is sufficient to induce TUJ1+ neurons (Figure S7H), and, upon NVOF expression, substantial numbers of progenitors lose progenitor features and acquire unipolar neuronal morphology by three days-post-transfection (Figure 2E). Further, and quite remarkably, over-expression of the SCPN/CSN-molecular control *Ctip2* (which has no known proneural function) in SOX6+/NG2+ progenitors is sufficient to induce unipolar neuronal morphology, TUJ1 expression, and down-regulation of glial genes (Figure S4F-4G). Together, these results indicate that SOX6+/NG2+ progenitors have substantial competence to differentiate into neurons, cortical projection neurons in particular, and that they are at a relatively advanced stage of progenitor fate acquisition.

Directed differentiation of type- or subtype-specific neurons from a developmentally related population of local progenitors might encounter fewer epigenetic blocks than with stem cell or less closely related progenitor populations, thus resulting in improved functional differentiation of type- or subtype-specific neurons. Recent studies have documented that residual transcriptional, epigenetic and chromatin domain signatures specific to cells of origin persist during derivation of iPSCs, e.g., especially during early passages[119-121]. Such bias and/or blockade is likely to be suboptimal for differentiation of functional type- or subtype-specific neurons, and thus for either functional regeneration or reliable modeling of pathology. Circumstantially supporting this view of persistent effects of cellular origin, reprogramming of fibroblasts to neuronal lineage occurs at a much lower efficiency and more slowly compared to reprogramming of cultured postnatal astrocytes[122], or to our results reported here. Intriguingly, we find that cortical SOX6+/NG2+ progenitors transfected with the single factor *Fezf2* acquire a hybrid morphology, preserving glia-like cell body morphology while developing a neuron-like, single, long primary neurite (Figure S4D and S4E). These results suggest incomplete and heterogenous neuronal induction. Since *Fezf2* has no known proneuronal function, and since it functions centrally in specification and differentiation of cortical output neurons with long axons, it is possible that some of the *Fezf2*'s target genes and their regulatory domains remain epigenetically accessible in cortical SOX6+/NG2+ progenitors. This partial, seemingly hybrid, differentiation driven by *Fezf2* alone further reinforces both the competency of SOX6+/NG2+ progenitors to differentiate relatively efficiently into cortical output projection neurons, and the need for multi-component regulation to guide cortical output projection neuron differentiation while suppressing alternative fates and enhancing cell type distinction.

Summary

The work reported here substantially and uniquely advances the goal of induction of neurogenesis and directed differentiation of subtype-specific neurons from endogenous adult progenitors. We first identify the SOX6+/NG2+ cortical progenitor population and employ genetic access to pure cultures of these progenitors. We then develop NVOF, a first-generation multi-component transcriptional regulatory construct, that induces cortical output neuron directed differentiation while suppressing the otherwise default glial differentiation pathway. We next identify that NVOF-directed neurons derived from SOX6+/NG2+ cortical progenitors differentiate with remarkable fidelity to *bona fide in vivo* cortical output neurons with appropriate morphological, molecular, deep transcriptomic, and electrophysiological characteristics. Further, these neurons do not display characteristics of inappropriate, alternative neuron types, most notably not even of closely related by non-output-neuron cortical projection neurons. This sharp subtype delineation is in striking contrast to previously developed approaches (e.g. fibroblast or iPSC-derived iNs, or glial-derived neuron-like cells) that generate much more "generic" neuron-like cells with mixed molecular identity, multipolarity, and often continued expression of some genes residual from the cells of origin, further confusing the output cellular identity[143-146]. Instead, SOX6+/NG2+ cortical

progenitor-derived neurons closely resemble corticospinal/subcerebral projection neurons with some hybrid corticothalamic molecular markers (the two dominant and developmentally closely related subtypes of the specialized cortical output neurons), reminiscent of the ~5% population of CSN/SCPN *in vivo* with hybrid corticothalamic molecular and projection features. Together, this developmentally based directed differentiation from genetically accessible, developmentally appropriate adult cortical progenitors sets a precedent and foundation for future optimizations of combinatorial levels, order, temporal dynamics, and subcellular localizations of an appropriate set of molecular controls over subtype-specific neuronal differentiation for *in vitro* mechanistic and therapeutic disease modeling, and toward regenerative neuronal repopulation and circuit repair.

Acknowledgements

This work was supported by NINDS grants NS045523, DP1 NS106665, and NS049553, and by grants from the Jane and Lee Seidman Fund for CNS Research, and the Emily and Robert Pearlstein Fund for Nervous System Repair (to J.D.M.). A.O. was partially supported by a fellowship from the Suna and Inan Kirac Foundation. H.P. was partially supported by an International Brain Research Organization Fellowship, and a McKnight Brain Research Institute/Regeneration Project Fellowship. We thank Jessica Kim, Jessica Wooten, Ioana Florea, and Ryan Humphries for technical assistance; David Dombkowski at MGH and Girijesh Buruzula, Joyce LaVecchio, and Silvia Ionescu at HSCRB for their help with FACS purification; Andrew Thompson for help with the cloning; Vibhu Sahni and Maria Galazo for assistance with retrograde labeling of SCPN/CSN and scientific discussions; Wataru Ebina for help with synthetic modified RNA experiments; Pratibha Tripathi for advice on astrocyte culture; and other members of the Macklis Laboratory for helpful suggestions and critical reading of the manuscript.

Author Contributions

J.D.M., H.P. and E.A. conceived of the project; J.D.M., A.O. and H.P. designed experiments with input from A.N.B.; A.O. and H.P. performed all culture experiments; P.K., C.S. and H.P. performed synthetic modified mRNA cloning; S.S. performed all electrophysiology recordings and analyzed these data; A.O., H.P. and J.D.M. analyzed and interpreted the data and wrote the manuscript. All authors read and approved the manuscript.

Materials and Methods

Mice

All mouse studies were approved by the Harvard University IACUC and were performed in accordance with institutional and federal guidelines. The date of vaginal plug detection was designated embryonic day (E) 0.5, and the day of birth as postnatal day (P) 0. Wild-type CD1 mice were purchased from Charles River Laboratories (Wilmington, MA). The NG2.DsRed.BAC mouse line was generated by Nishiyama and colleagues[66], and was procured from Jackson Laboratories (stock number: 008241). *Sox6* knockout mouse was the generous gift of V. Lefebvre (Cleveland Clinic)[147], and was maintained on c57bl/6 background and separately crossed into an outbred CD1 background. Most *Sox6* knockout embryos on a c57 background die perinatally[60], while outcrossing into the CD1 background resulted in live *Sox6* knockout pups. These pups survived for several days, developed poor body condition, and died by about P14. Male and female pups were included in all retrolabeling, FACS purification, and culture experiments. All mice were maintained in standard housing conditions on a 12-hour light/dark cycle with food and water ad libitum. A maximum of four adult animals were housed per cage.

BrdU Labeling

To cumulatively label dividing cells in the cortex at P7 and P28, BrdU (Sigma, B5002) was injected intraperitoneally from P3 to P7 or from P23 to P28 (50 µg/mg/injection). To cumulatively label slowly dividing and/or quiescent populations in adult brain, BrdU was added to drinking water for 4-6 weeks (1.5 mg/mL). Brains were collected at corresponding ages and processed for BrdU immunocytochemistry.

Plasmids

CMV/ß-actin promoter-driven plasmid pCBIG (derived from CBIG, a gift from C. Lois, Caltech) was used to drive expression of IRES-Gfp (control), single factors (*Ctip2*, *Neurog2*, *VP16:Olig2*, *Fezf2-HA*, and tdTomato) or NVOF construct. The NVOF construct was created by cloning GFP, *Neurog2*, *VP16-Olig2*, and *Fezf2-HA* coding sequences separated by 2A linker sequences into a pCBIG vector. In this system, genes linked to each other via viral 2A sites are transcribed as a single mRNA, but are translated into individual polypeptides[72,148,149]. For synthetic modified mRNA synthesis, GFP, RFP, *Fezf2-HA*, and *Neurog2* open reading frames were cloned into pORFin or pORFinB vectors (from D. Rossi Lab, HSCRB and Boston Children's Hospital). pORFin vectors had the appropriate 5' and 3' UTR sequences flanking the cloning sites, and an upstream T7 promoter for *in vitro* transcription. RNA was synthesized in accordance with a published protocol[150].

Purification and Culture of Cortical SOX6+/NG2+ Progenitors

Heterozygous offspring pups (P2-P5) from the NG2-DsRed male and wild-type CD1 female crosses were used for FACS experiments. Pups were screened for red fluorescence under a dissecting microscope (Nikon, SMZ-1500), and anesthetized on ice. Brains were dissected, and meninges were removed in ice-cold Hank's buffered salt solution (HBSS) (Gibco, 14025092). Neocortices were micro-dissected in ice-cold dissociation medium (pH 7.35), composed of 20 mM glucose (Sigma, G6152), 0.8 mM kynurenic acid (Sigma, K3375), 0.05 mM DL-2-amino-5-phosphonopentanoic acid (APV) (Sigma, A5282), 100 U/ml penicillin - 100 µg/ml streptomycin (Gibco, 15140122), 0.09 M Na_2SO_4, 0.03 M K_2SO_4, and 0.014 M $MgCl_2$ (pH 7.35±0.02). Dissected cortices were enzymatically digested in dissociation medium containing 0.16 mg/ml DL-Cysteine hydrochloride (Sigma, C9768), 10 U/ml papain (Worthington, LS003126), and 30 U/ml DNAse I (Sigma, D5025) at 37 °C for 30 minutes, rinsed two times with ice-cold OptiMEM (Gibco, 51985034), and supplemented with 20 mM glucose, 0.4 mM kynurenic acid, and 0.025 mM APV to protect against glutamate-induced neurotoxicity[151]. Digested cortices were mechanically dissociated by gentle trituration using fire-polished glass Pasteur pipets to create a single-cell suspension. Dissociated cells were centrifuged at 100 g for 5 minutes at 4 °C, resuspended (5-10x10^6 cell/ml) in OptiMEM with supplements, and filtered through a 35 µm cell strainer (Corning, 352235). All chemicals were purchased from Sigma-Aldrich unless stated otherwise.

Cells were purified based on DsRed fluorescence intensity using a BD FACSAria II cell sorter in four-way purity mode (85 µm nozzle). DsRed-positive cells from the NG2.DsRed BAC-transgenic mouse cortex consisted of two distinct populations: bright and dim. After qPCR and immunocytochemical characterization of both populations, only the bright population, which yielded 200-300K cells/brain, was purified for induced neurogenesis experiments. A previously published protocol was adapted to maintain cells in a proliferative progenitor state[152]. Purified cells were sorted into and cultured in growth medium, composed of DMEM/F12 with GlutaMAX (Gibco, 10565018), 15 mM HEPES (Gibco, 15630106), B27 without vitamin A (Gibco, 12587-010), N2-max (R&D Systems, AR009), 100 U/ml penicillin - 100 µg/ml streptomycin (Gibco, 15140122), 10 ng/ml PDGF-A (Peprotech, 315-17), and 20 ng/ml FGF2 (Peprotech, 450-33). Half of the medium in each well was replaced every other day. Cells were seeded (~10K cells/cm^2) on either 50-100 µg/ml poly-D-lysine (Sigma, P0899) plus laminin (Thermo, 23017015), or 0.01% poly-L-ornithine (Millipore, A-004-C) plus laminin-coated cover glasses (Fisher, 12-545-81) in 24-well plates for microscopy experiments (Corning, 353047), or without cover glass in 6-well plates for RNA experiments (Corning, 353047). Transfection was performed at ~5 DIV after half-replacing the medium with fresh proliferation medium using Fugene 6 (Promega) with the following ratio: per 6-well plate, 600 µl DMEM/F12 medium (w/o supplements), 30 µl transfection reagent, and 8 µg of DNA was mixed, incubated for 15-30 minutes, and directly added into each well (~100 µl/well), yielding ~10% transfection rate at 24 hours. The same Fugene 6 transfection reagent was used for synthetic RNA transfections (20 µl media, 1.2 µl transfection reagent, and 0.2 µg RNA for each well of the 24-well plate). On the day following transfection, growth medium was replaced with neuronal induction medium, composed of a 1:1 mixture of DMEM/F12 and Neurobasal-A (Gibco, 10888022), GlutaMAX (Gibco, 35050061), 15 mM HEPES, B27 with vitamin A (Gibco, 17504044), N2 (Gibco, 17502048), and

100 U/ml penicillin - 100 μg/ml streptomycin (Gibco, 15140122). Medium was half-replaced every third day after transfection until fixation.

Retrograde Labeling and FACS Purification of SCPN and CPN

Retrograde labeling experiments were adapted from previously published procedures[47]. Briefly, pups were anesthetized by hypothermia at P0/P1, and SCPN and CPN were retrolabeled from their corresponding axonal projections by pressure injection (Nanoject II, Drummond) of Alexa Fluor 555-conjugated cholera toxin, subunit B (CTB) (Invitrogen, C22843) (6-7 injections, 23 nl/injection, 2 μg/ul) using pulled and beveled glass micropipettes with a tip diameter of 30–50 μm. SCPN were labeled from the cerebral peduncle, and CPN were labeled from contralateral corpus callosum close to the midline (3-4 rostrocaudal levels). Injections were performed in deeply anesthetized pups using a Vevo 770 ultrasound backscatter microscopy system (VisualSonics). Brains were collected at P2 for FACS purification, and retrograde labeling success was verified under a fluorescence-equipped dissecting microscope (SMZ-1500; Nikon). Cells were purified with stringent fluorescence gating using a BD FACSAria II cell sorter (85 μm nozzle) in four-way purity mode.

In utero Electroporation

Timed pregnant CD1 dams were anesthetized with isoflurane, and an incision was made in the abdomen. The uterine horns were exposed and gently positioned on a sterile piece of gauze. 1.0 μg/μl of plasmid DNA was mixed with 0.005% Fast Green in sterile PBS and injected *in utero* into one lateral ventricle of each embryonic brain. The injections were performed with beveled glass micropipettes (tip diameter of 30–60 um) via mouth pipetting with an aspirator tube assembly (Sigma, A5177). Plasmid electroporations were performed by placing a positive electrode (tweezer electrodes, 5 mm diameter) above the cortex and a negative electrode behind the head, and applying five pulses of current at 40V for 50 milliseconds per pulse with 1 second intervals between pulses (CUY21Edit Electroporator, Bex Co. Ltd.). Brains were collected at P7 for NVOF misexpression analysis and at P0-P1 for primary neuron culture.

Astrocyte-conditioned Media

Production of astrocyte-conditioned media was based on the published protocol for primary culture of postnatal cortical astrocytes[153]. Briefly, cerebral cortices were micro-dissected from wild-type P5-P7 CD1 pups, gently dissociated without enzymatic digestion using fire-polished glass Pasteur pipets, and centrifuged at 100 g for 5 minutes at 4 °C. Dissociated cells were seeded in T25 flasks, and cultured in astrocyte growth medium (DMEM/F12 with GlutaMAX (Gibco, 10565018), 10% fetal calf serum (Seradigm, 97068-091), 5% horse serum (Invitrogen, 26050070), B27 (with vitamin A), 100 U/ml penicillin – 100 μg/ml streptomycin (Gibco, 15140122), 10 ng/ml EGF (Peprotech, 315-09), and 10 ng/ml FGF2 (Peprotech, 450-33). Medium was fully changed 24 hours post-culturing, and half of the medium was replaced three days post-culturing. Culture fidelity was verified by morphology and GFAP expression of the differentiated cells. To obtain astrocyte-conditioned media, astrocytes were passaged at ~5 DIV using trypsin (Gibco, 25200056), centrifuged at 100 g for 5 minutes at room temperature, diluted 1:4, re-seeded in T75 flasks containing astrocyte growth medium, and cultured for 24 hours. Growth medium was subsequently replaced with neuronal induction medium (described above). The conditioned medium was collected at days 10, and 20, and aliquots were stored at -80°C.

NVOF-induced and primary neuron co-culture

To co-culture of induced neurons with primary neurons, primary forebrain neurons were obtained from P0-P1 CD1 wild-type pups using the dissociation protocol described above, and directly added onto progenitor cell cultures at 24 hours after transfection (25K/cm^2). One half of the medium was replaced with fresh astrocyte-conditioned media every third day. For dendritic morphology comparison, cortical projection neurons were labeled via *in utero* electroporation (at E14.5) of a tdTomato reporter plasmid driven by CMV-beta-actin promoter (see above). Neurons were dissociated at P0-P1, cultured in 24-well plates with cover glass (50K cell/cm^2), and cultured in parallel with induced neurons using the same neuronal media that is described above.

Histology and Immunocytochemistry

Immunocytochemistry (ICC) for tissue sections was performed following standard protocols. Briefly, mice were transcardially perfused with PBS then 4% PFA, dissected, and post-fixed overnight at 4 °C in 4% paraformaldehyde. Brains were embedded in 4% low melting temperature agar (Sigma-Aldrich) and sectioned at 50 μm on a vibrating microtome (Leica). Fixed tissues were stored in PBS with 0.025% sodium azide. Floating sections were blocked with 0.3% BSA (wt/vol) (Sigma, A3059), 0.3% Triton X-100 (Sigma, T8787), and 0.025% sodium azide (Sigma, S2002) in PBS for 30 minutes. Primary antibodies were diluted in the same blocking solution and incubated with sections for 4 hours at room temperature, or overnight at 4 °C. Sections were rinsed three times with PBS for 10 minutes and incubated with appropriate secondary antibodies diluted in blocking solution for 2-3 hours at room temperature. Sections were rinsed three times with PBS, and mounted using Fluoromount with DAPI (SouthernBiotech, 0100-20) for image acquisition. ICC for BrdU was preceded by 2 hours of treatment with 2 N HCl at room temperature for antigen retrieval.

ICC for cultured cells was performed by first fixing cells in 4% paraformaldehyde at room temperature for 10 minutes, rinsing three times with PBS, and storing in PBS with 0.025% sodium azide at 4 °C. Cells were blocked in the blocking solution for 15 minutes, incubated with primary antibodies for 2 hours, rinsed with PBS three times for 5 minutes, incubated with secondary antibodies for 45 minutes, rinsed with PBS three times for 5 minutes (all reactions at room temperature), and mounted using Fluoromount with DAPI.

The following primary antibodies and dilutions were used: mouse anti-ANK3 (ANKYRIN-G), 1:250 (Santa Cruz, sc-12719); rat

anti-BrdU, 1:500 (ACSC, OBT0030); rabbit anti-CSPG4 (NG2), 1:500 (Millipore, AB5320); rabbit anti-CTIP2, 1:500 (Abcam, ab28448); rat anti-CTIP2, 1:250 (Abcam, ab18465); rabbit anti-CUX1, 1:200 (Santa Cruz Biotechnology, sc-13024); rabbit anti-DARPP32, 1:250 (Cell Signaling Technology, 2306S); rabbit anti-FOG2, 1:250 (Santa Cruz Biotechnology, sc-10755); rabbit anti-FOXP2, 1:2000 (Abcam, AB16064); mouse anti-GABA, 1:200 (Sigma, A0310); mouse anti-GFAP, 1:1000 (Sigma, G3893); rabbit anti-GFAP, 1:1000 (Sigma, G9269); chicken anti-GFP, 1:1000 (Invitrogen, A10262); rabbit anti-GFP, 1:1000 (Invitrogen, A11122); mouse anti-HA, 1:1000 (Covance, MMS-101R); mouse anti-ISL1, 1:250 (Novus, H00003670); mouse anti-MAP2, 1:500 (Sigma, M1406); chicken anti-NESTIN, 1:2000 (Novus, NB100-1604); mouse anti-NeuN, 1:500 (Chemicon, MAB377); rabbit anti-NF-M, 1:200 (Millipore, AB1987); mouse anti-NEUROG2, 1:100 (R&D Systems; MAB3314); goat anti-OLIG2, 1:200 (R&D Systems, AF2418); rat anti-RFP, 1:500 (antibodies-online, ABIN334653); rabbit anti-PCP4, 1:500 (Proteintech, 14705-1-AP); rabbit anti-PDGFRB, 1:100 (Cell Signaling, 3169); mouse anti-PSA-NCAM, 1:200 (Chemicon, MAB5324); mouse anti-SATB2, 1:200 (Abcam, ab51502); rabbit anti-SATB2, 1:500 (Abcam, ab34735); rabbit anti-SOX6, 1:500 (Abcam, AB30455); goat anti-SOX10; 1:200 (Santa Cruz, sc-17342); rabbit anti-SYNAPSIN, 1:500 (Synaptic Systems, 106002); mouse anti-SYNAPTOPHYSIN, 1:500 (Millipore, MAB5258); rabbit anti-TH, 1:250 (Millipore, AB152); rabbit anti-TUBB3 (Tuj1), 1:1000 (Sigma, T2200); mouse anti-TUBB3 (Tuj1), 1:1000 (Biolegend, MMS-435P), rabbit anti-vGLUT1, 1:500 (Synaptic Systems, 135302); rabbit anti-2A-peptide, 1:1000 (Millipore, ABS31), rabbit anti-5HT, 1:3000 (Immunostar, 20080). Alexa Fluor-conjugated secondary antibodies (Invitrogen) were used at a dilution of 1:1000. Positive controls were included in all ICC experiments with negative results. All ICC experiments utilized different batches of FACS-purified cells from independent litters to yield a minimum of three true biological replicates. Primary data were analyzed by one investigator (AO), then confirmed by a second independent investigator (HP).

Image Acquisition, Quantification, and Statistical Analysis

Wide-field image acquisition was performed with a Nikon 90i epifluorescence microscope equipped with a Clara DR-328G cooled CCD digital camera (Andor Technology) running NIS Elements software (Nikon). Brightfield images were acquired using a Nikon ECLIPSE Ts2R-FL inverted microscope. For optimal data visualization, images were adjusted for contrast, brightness, and size in Adobe Photoshop and Illustrator (2019). Identical procedures were applied across different experimental conditions. For cell quantifications, a cover glass area of ~50 mm^2 (7x7 tile) was imaged using a 10x objective. The acquired image was binned as 1 mm^2 boxes, individual boxes were randomly selected, and all GFP+ cells in each selected box were quantified using NIS-elements software (Nikon). To quantify the immunofluorescence intensity of target molecules, nuclei were identified via DAPI, and the average intensity of the outlined nuclear area was measured on Nikon-NIS. The following criteria were used to mark neurons with multiple axons: If the second longest neurite originating from the cell soma was at least half the length of the longest neurite, that cell was marked as multipolar. A minimum of four independent biological replicates were used for each experimental condition across the study unless otherwise mentioned in the text. Microsoft Excel, RStudio (version 1.3.959), and GraphPad Prism 8 were used for data analysis, plotting graphs, and statistics. Statistical details of the experiments can be found in the figure legends. Significance is based on the p value indicated on the graphs as * p % 0.05, ** p % 0.01, ***p % 0.001, ****p % 0.0001.

Electrophysiology

Electrophysiological recordings were performed at 20-25 °C on an Olympus BX51WI microscope. Cells were bathed in artificial cerebral spinal fluid (ACSF) containing 119 mM NaCl, 2.5 mM KCl, 4 mM $CaCl_2$, 4 mM $MgSO_4$, 1 mM NaH_2PO_4, 26.2 mM $NaHCO_3$, and 11 mM glucose. ACSF was continuously saturated with 95% O_2/5% CO_2. Intracellular recordings were obtained using glass micropipettes filled with an internal solution containing 136 mM $KMeSO_3$, 17.8 mM HEPES, 0.6 mM $MgCl_2$, 1 mM EGTA, 4 mM Mg-ATP, and 0.3 mM Na-GTP. Traces were collected using a Multiclamp 700B amplifier (Molecular Devices), filtered with a 2 kHz Bessel filter, digitized at 50 kHz using a Digidata 1440A digitizer (Molecular Devices), stored using Clampex 10 (Molecular Devices), and analyzed off-line via customized procedures written in Igor Pro (WaveMetrics). Series resistance was monitored throughout the experiment. Cells at DPI/DIV 15-16 were identified visually by fluorescence. Action potentials were evoked by injection of current steps, ranging from –140 pA to 400 pA in 60-pA increments, with a duration of 600 ms. Action potential parameters were quantified for the first action potential evoked at the lowest current injection that resulted in an action potential. The threshold potential was defined as the voltage at which dV/dt of the action potential waveform reached 10% of its maximum value, relative to a dV/dt baseline taken 10 ms before the peak. Action potential amplitude was defined as the difference between the threshold value (in mV) and the maximum voltage of the action potential. Width was measured at half-maximum amplitude. Sag current was measured during a -140 pA step current for a duration of 600 ms.

RNA sequencing

A minimum of three independent biological replicates was used for each experimental group (i.e., mouse litters, cell culture batches, FACS purifications, etc. were different for each biological replicate). RNA isolation was performed using a Qiagen RNeasy Plus Mini Kit with the gDNA elimination step. FACS-purified cells were collected directly into RLT Plus buffer with ß-mercaptoethanol. RNA concentration, purity, and integrity were measured by a Nanodrop (ThermoFisher), an Agilent TapeStation 2200, and an Agilent Bioanalyzer 2100. Only high-quality RNA samples were used for library preparation. For the 32 samples used in this study, the minimum RNA integrity number (RIN) was 8, the average was 9.7, and the median was 10.

Library preparation and sequencing were performed by the Bauer Core Facility at Harvard University. RNA was fragmented at 94 °C for 6 minutes with a final size range of 200-300 bp. The

library was prepared from 50 ng total input RNA per sample using a Kapa mRNA HyperPrep kit (14 cycles) with PolyA enrichment (stranded via dUTP addition, and first-strand preserved). Unique dual 8 bp adapters (1.5 μM) (IDT for Illumina) were used for indexing. The library quality and concentration were confirmed by an Agilent TapeStation 2200 and a Kapa qPCR library quantification kit. The pooled samples were run on Illumina NextSeq High flow cells (75bp, paired-end reading). Sequencing quality was assessed by FASTQC (version 0.11.9). STAR-aligned counts were used for quality control metrics[154].

The quasi-aligned counts from Salmon with default options were used to perform downstream gene expression analyses[155]. Transcript-level count matrices were produced via the Bioconductor package "tximport"[156]. Ensembl gene IDs were generated using the GRCm38 reference genome (Ensembl v98). DESeq2 was used to perform differential expression analyses[157]. Low count genes (total reads <10) were pre-filtered before DESeq2 functions. Gene names and other information were annotated using the Bioconductor package "AnnotationDbi". Variance-stabilizing transformed (vst) normalized counts (log2 scale) were used for data visualization[158]. The code used to perform subsequent analyses of the sequencing data was an adaptation of standard R packages. More detailed information is available upon request. Gene ontology (GO) enrichment analysis was performed using the PANTHER online database[159,160]. Raw FASTQ files and processed counts are available upon request.

Quantitative PCR

cDNA was prepared using the Superscript IV first-strand synthesis system (Thermo, 18090050) and random hexamers (Thermo, SO142) following the manufacturer's standard protocol. Random hexamers were used for amplification. qPCR was performed using the iTaq Universal Sybr Green Supermix (Bio-Rad) on a BioRad CFX96 thermal cycler following standard procedures. For all qPCR primers used in this study, reaction efficiency was calculated by standard curve analysis, and only primers with high efficiency (90-105%) were used. See Supplementary Table S2 for the primer list. Four independent biological replicates were used for each experimental group in all qPCR experiments.

Supplementary Table 1: Transcript counts for top-500 genes enriched in major cell lineages[63] and mural cells[161] for acutely sorted DsRed-Negative, -Dim, and -Bright cells, as well as cultured DsRed-Bright cells (5-DIV). Counts are variance-stabilizing transformed (vst) normalized data in log2 scale.

Supplementary Table 2: List of primer sets used in qPCR experiments.

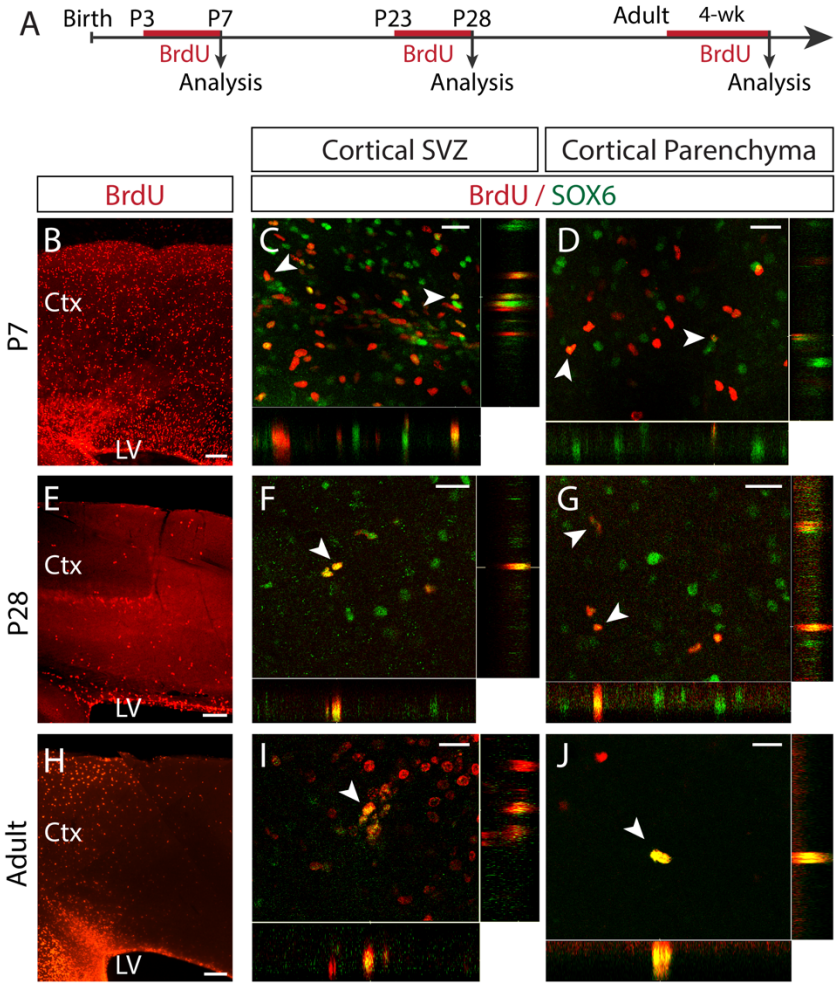

Figure S1. Identification of SOX6+ cortical progenitors in postnatal and adult neocortex

(A) Schematic of BrdU cumulative labeling experiments.
(B-D) Confocal photomicrographs of cortex sagittal sections showing BrdU+ proliferative cells at P7 (B), a subset of which express *Sox6* in the caudal cortical SVZ and cortical parenchyma (C and D). BrdU was injected from P3 to P7 in wild-type c57bl/6 mouse (50 µg/mg of body weight).
(E-G) Same experiment as (B-D), but BrdU administration is from P23-P28. Fewer BrdU-labeled cells are labeled in P28 neocortex (E), subset of which express SOX6 (F and G).
(H-J) After five-week administration of BrdU in drinking water, SOX6+/BrdU+ cells are identified in adult brain.
Scale bars (A, D, G) 150 µm; (B, C, E, F, H, I) 25 µm. Ctx: cortex, LV: lateral ventricle, SVZ: subventricular zone, P: postnatal-day, BrdU: Bromodeoxyuridine.

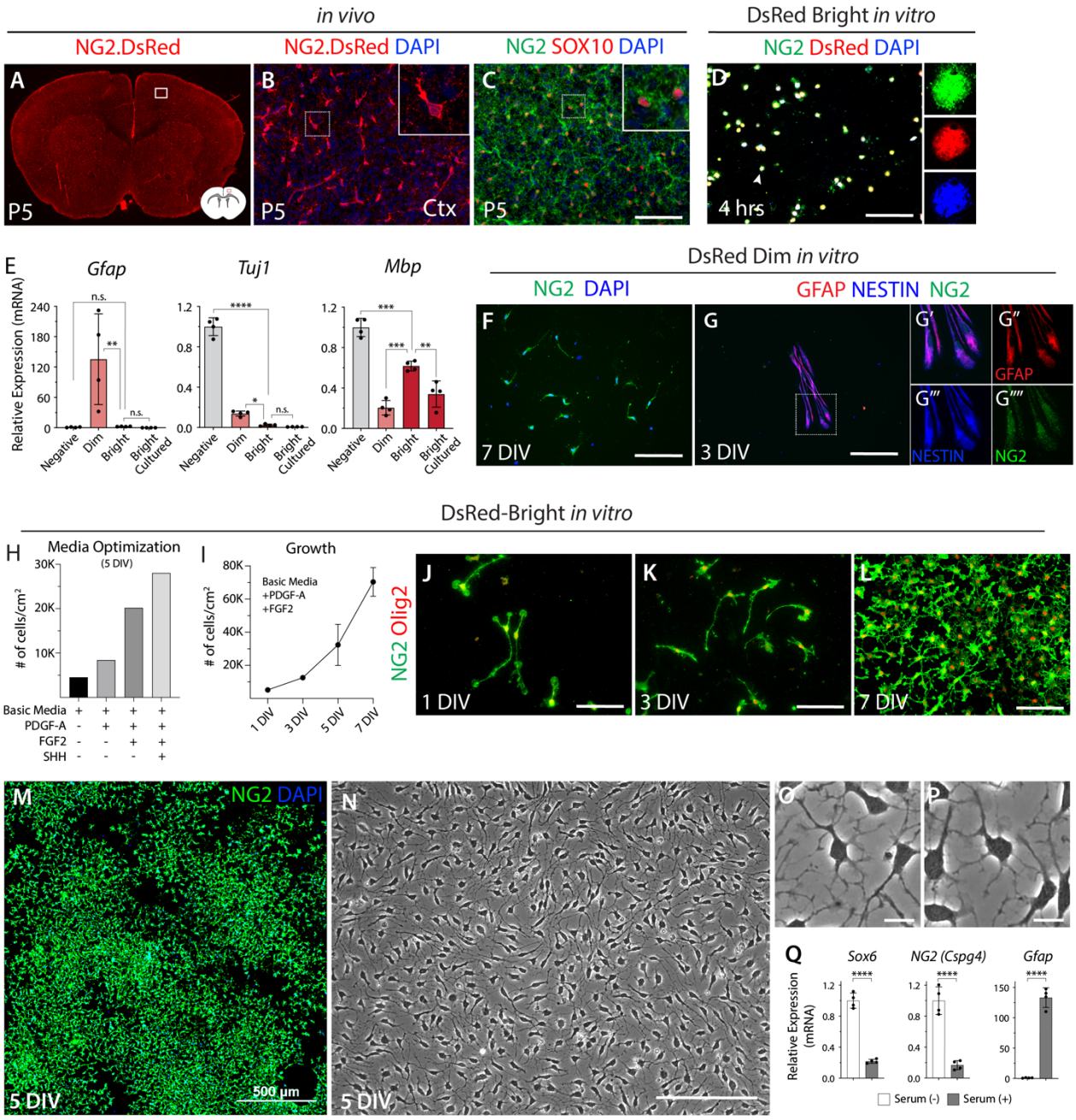

Figure S2. Characterization, FACS isolation, and culture of cortical SOX6+/NG2+ progenitors

(A-B) Photomicrograph of NG2-DsRed coronal section at P5 showing expression of DsRed by uniformly distributed progenitor cells and pericytes (see also Figures S3H-S3L). Schematic in A depicts a coronal section; boxed region in A identifies the approximate region shown in B. Ctx: cortex.

(C) Immunostaining of NG2 and SOX10 shows uniform distribution of NG2+ progenitors in cortex at P5.

(D) Immunostaining confirms expression of NG2 and DsRed by cultured DsRed-Bright cells after FACS purification (4 hours). n=2, biological replicates.

(E) qPCR of *Gfap*, *Tuj1*, and *Mbp* demonstrates that acutely sorted and cultured DsRed-Bright cells do not contain neurons or astrocytes, and that culture conditions do not promote oligodendrocyte differentiation. n=4, biological replicates, *Actb* normalized data relative to negative population.

(F-G) Immunofluorescence shows that DsRed-Dim populations contain a mixture of NG2+ cells (with relatively low NG2 expression compared to DsRed-Bright; see S2L) (F) and GFAP+/NESTIN+/NG2+ glial progenitors (G).

(H) Quantification of progenitor proliferation in response to PDGF-A, FGF2, and SHH at 5 DIV. (Due to potential ventralization by SHH, only PDGF-A and FGF2 were used in subsequent experiments.)

(I) Cultured SOX6+/NG2+ cortical progenitors proliferate robustly in response to PDGF-A and FGF2. Cell number increases 7-fold through 7 DIV. n=2, biological replicates.
(J-L) Representative images of cultured progenitors shows proliferation and continued expression of NG2 and Olig2 over time.
(M and N) Low-magnification immunofluorescence and bright-field images of progenitors in culture show expression of NG2 proteoglycan, and maintenance of multipolar morphology through 5 DIV.
(O-P) Representative high-magnification (40x) images of progenitors in culture shows preservation of characteristic non-overlapping processes by SOX6+/NG2+ progenitors.
(Q) qPCR shows that serum causes cultured progenitors to decrease expression of the key progenitor genes *Sox6* and *NG2*, and increase expression of the astroglial marker *Gfap*. n=4, biological replicates, *Actb* normalized data relative to negative population.
Scale bars (C, D, F, G, J, K, L, N) 100 µm, (M) 500 µm, (O, P) 10 µm. Data are presented as mean ± SD. ****$p < 0.0001$, ***$p < 0.001$, **$p < 0.01$, *$p \geq 0.05$, no statistically significant difference (n.s.); ANOVA Tukey's post hoc test in (E), t-test in (Q).

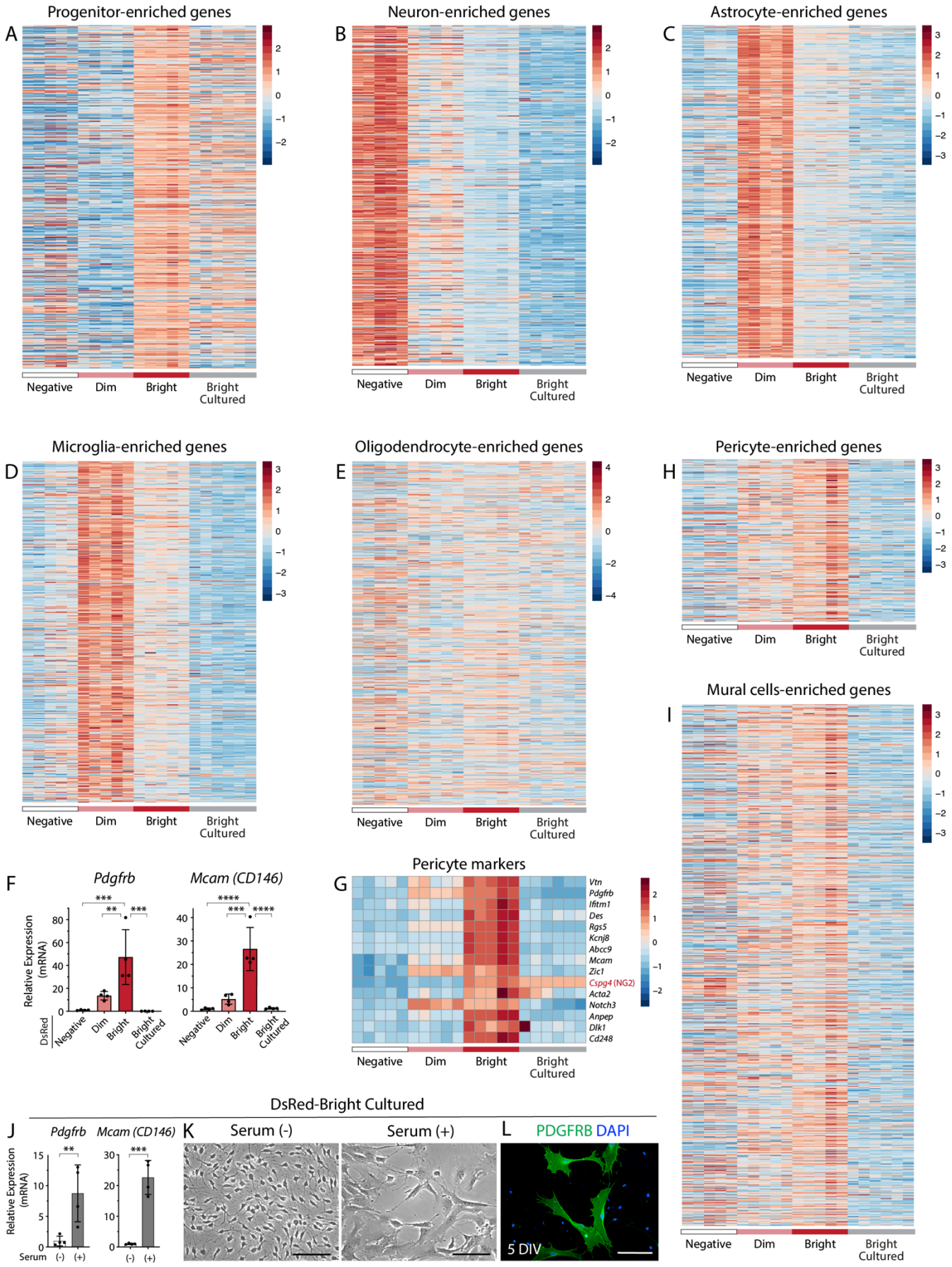

Ozkan*, Padmanabhan* et al., 2024 (preprint)

Figure S3. SOX6+/NG2+ progenitors maintain molecular characteristics *in vitro,* and cultures are free of DsRed+ pericytes

(A-E) Heatmap of the top-500 genes enriched in major cell lineages[63] for acutely sorted DsRed-Negative, -Dim, and -Bright cells, as well as cultured DsRed-Bright cells (5-DIV). Counts are variance-stabilizing transformed (vst) normalized data in log2 scale.
(F) qPCR of the pericyte markers *Pdgfrb* and *Mcam (CD146)* shows that pericytes are FACS-purified with SOX6+/NG2+ progenitors in DsRed-Bright populations, but they are not present in culture at 5 DIV. Data are presented as mean ± SD, n=4, biological replicates, *Actb* normalized data relative to negative population.
(G-I) Heatmaps of commonly known pericyte markers (G), a conservative list of 241 pericyte-enriched genes (H), and an extended list of 785 genes that are enriched in brain mural cells (I)[161], confirming absence of pericytes in culture. See Supplementary Table S1 for a list of genes used in these plots.
(J-L) qPCR (J), microscopy (K), and immunocytochemistry (L) of DsRed-Bright cells cultured in standard proliferation media with or without serum (see methods) at 5 DIV showing that pericytes only survive in the presence of serum. qPCR data are presented as mean ± SD, n=4, biological replicates, *Actb* normalized data relative to no serum condition.
Scale bars (K) 50 µm, (L) 100 µm. ****$p < 0.0001$, ***$p < 0.001$, **$p < 0.01$; ANOVA Tukey's post hoc test in (F), t-test in (J).

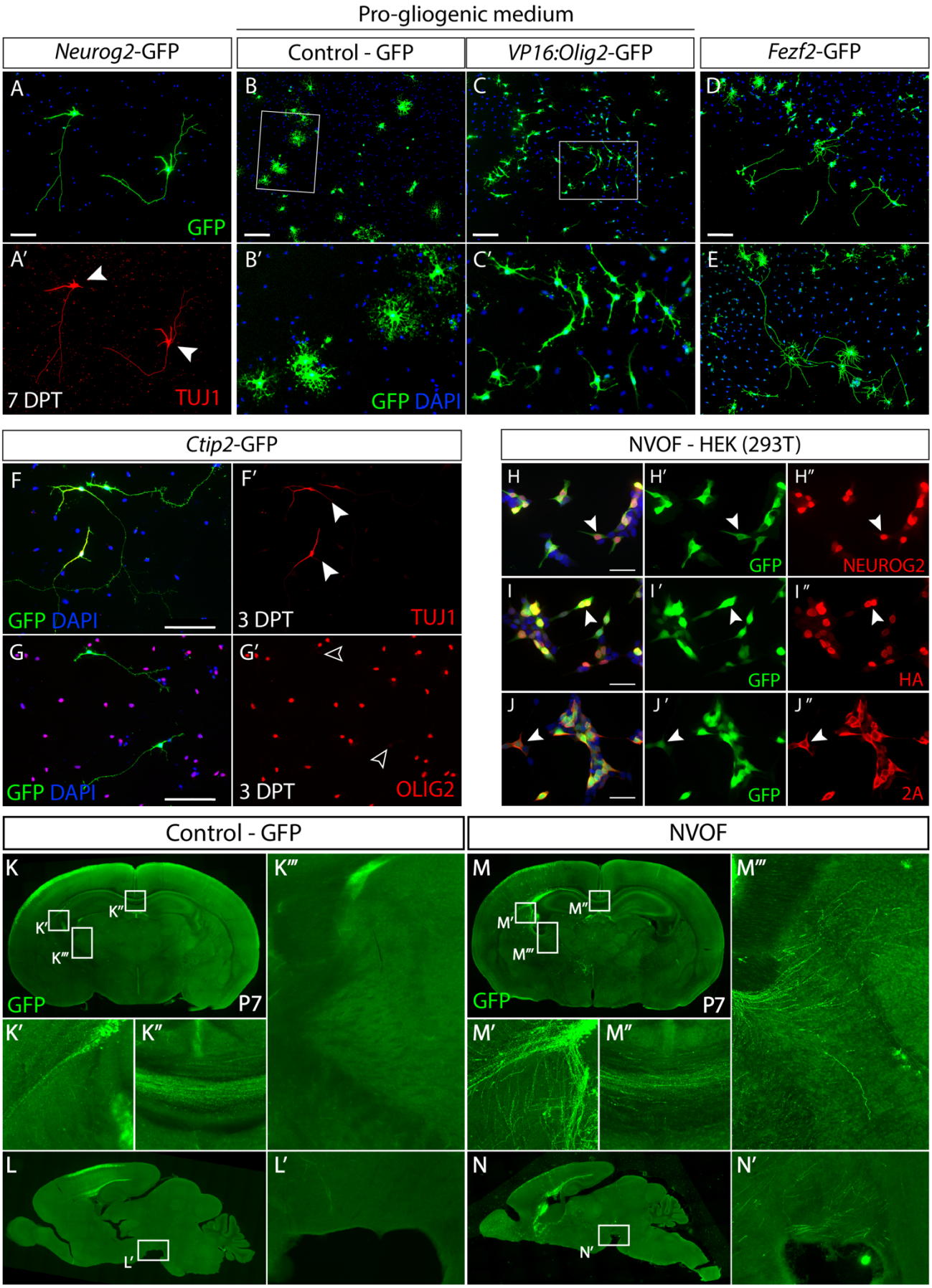

Ozkan*, Padmanabhan* et al., 2024 (preprint)

Figure S4. Expression and function of individual NVOF components

(A) Representative image of *Neurog2*-GFP-induced neurons showing TUJ1 expression (A').
(B, C) Representative images of control-GFP versus *VP16:Olig2*-GFP-transfected SOX6+/NG2+ progenitors. Overexpression of *VP16:Olig2* represses T3-mediated differentiation of progenitors into oligodendrocytes, causing transfected cells to acquire morphology of immature neuroblasts (n=3).
(D, E) Representative images of *Fezf2*-GFP transfected cells. *Fezf2* overexpression in progenitors does not fully support neuronal differentiation, and many cells adopt a 'chimeric' morphology with glial-cell-like soma structures and long processes. (n=2)
(F, G) Representative images of *Ctip2*-GFP transfected cells. *Ctip2* overexpression in SOX6+/NG2+progenitors induces a striking, TUJ1+/OLIG2- axon-like neurite at 3 DPT, demonstrating inherent plasticity and neuronal competency in SOX6+/NG2+ progenitors.
(H-J) Immunofluorescence of HEK293 cells transfected with NVOF confirms that GFP, NEUROG2 (H), and FEZF2-HA (I) are expressed appropriately. Immunocytochemistry for 2A peptides reports expression of GFP, NEUROG2, and VP16:OLIG2 (J).
(K-N) Testing NVOF in embryonic dorsal progenitors at E15.5 via *in utero* electroporation. E15.5 embryos were electroporated with control vector (GFP) (K, L) and NVOF (M, N), and analyzed at P7. Neurons electroporated with control vector project to contralateral cortex (K"), but not to subcortical targets (K', K''', L'). After NVOF electroporation, many GFP+ axons descend through internal capsule (M') towards thalamus (M'''), and some of these axons even reach cerebral peduncle by P7 (N). Some NVOF-electroporated neurons still send axons to contralateral hemisphere through the corpus callosum (M"). Together, these data show that NVOF redirects axons of later-born upper-layer neurons from contralateral targets to subcortical targets, akin to deep-layer cortical output neurons. (n=4)
Scale bars (A-G) 100 μm; (H-J) 50 μm.

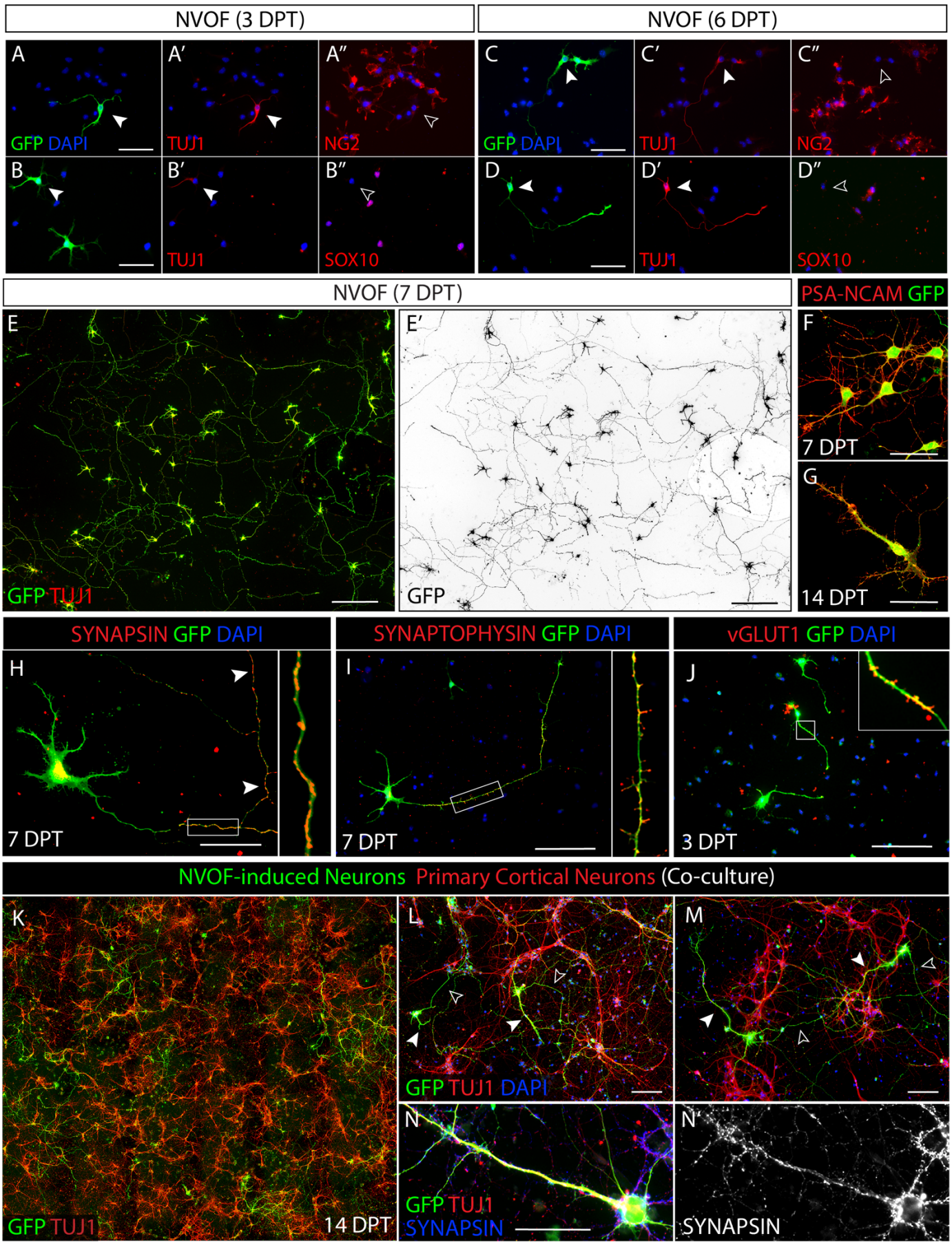

Ozkan*, Padmanabhan* et al., 2024 (preprint)

Figure S5. NVOF-transduced progenitors rapidly lose progenitor identity and acquire cardinal features of mature functional neurons

(A-D) Representative images of NVOF-transfected progenitors at 3- and 6 DPT showing acquisition of neuronal morphology coupled with TUJ1 expression (filled arrows) and downregulation of the progenitor markers NG2 (a.k.a. *Cspg4*) and SOX10 (empty arrows).
(E) Representative low-magnification image of NVOF-induced neurons at 7 DPT. (E') Pseudocolored GFP for better visualization of cell morphology.
(F-J) NVOF-induced neurons at 7 DPT express the cell adhesion molecule PSA-NCAM (F), which has a punctate distribution at 14 DPT (G), and the presynaptic molecules SYNAPSIN (Syn1/2) (H), SYNAPTOPHYSIN (Syp) (I) and VGLUT1 (J), which are key molecular features of glutamatergic neurons. Note the localization of SYNAPSIN and VGLUT1 to filopodial, presumptive presynaptic structures along axonal compartments.
(K) Representative low-magnification image of NVOF-induced neurons (green, GFP) co-cultured with primary neurons isolated from wild-type forebrain at P0 (red, Tuj1) in astrocyte-conditioned media, showing that NVOF-induced neurons intercalate with primary neurons at 14 DPT.
(L, M) Representative images of co-culture showing considerable morphological maturation and axon elongation of NVOF-induced neurons. Note dendrite size (filled arrows) and single axons protruding from cell bodies (empty arrows).
(N) Representative image of an NVOF-induced neuron with highly elongated dendritic structures, and abundant SYNAPSIN-positive presynaptic contacts from nearby primary neurons (N').
Scale bars (A, B, C, D, I, J, L, M) 100 μm; (E) 200 μm; (F, G, H, N) 50 μm.

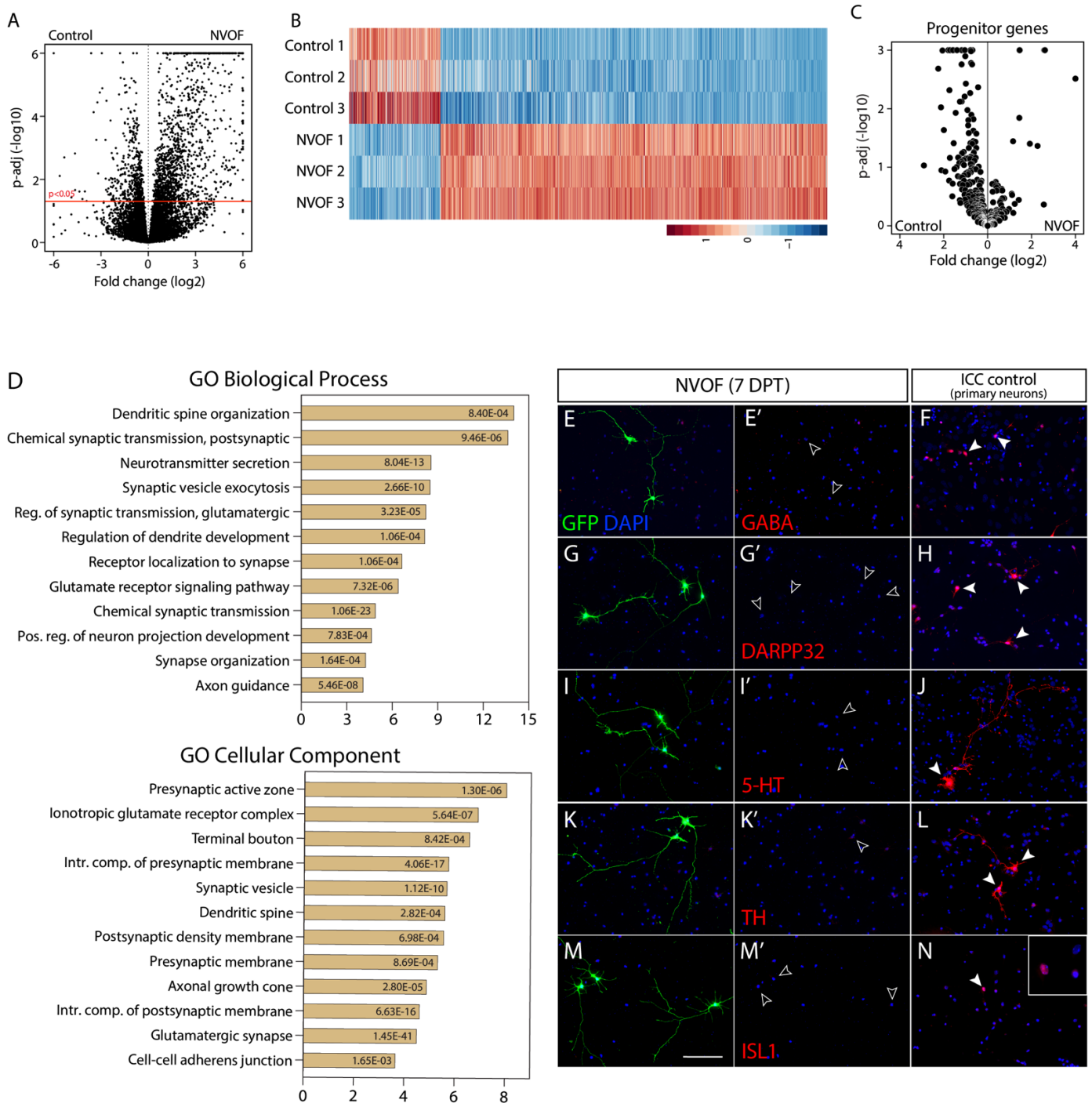

Figure S6. NVOF induces glutamatergic neurons from SOX6+/NG2+ progenitors with high fidelity and reproducibility.

(A, B) Volcano and heatmap of differentially expressed genes between NVOF-induced neurons and cells transfected with control-GFP.
(C) Volcano plot showing downregulation of progenitor genes in NVOF-induced neurons compared to control-GFP transfected cells at 7 DPT (n=3, biological replicates).
(D) Gene ontology (GO) term enrichment analysis of genes upregulated in NVOF-induced neurons for biological processes and cellular components.
(E-M) Representative images of NVOF-induced neurons with negative immunoreactivity for the non-glutamatergic neuronal markers GABA for GABAergic interneurons (E, E'), DARPP32 for striatal projection neurons (G, G'), 5-HT for serotonergic neurons (I, I'), TH for dopaminergic neurons (K, K'), and ISL1 for spinal motor neurons (M, M'), demonstrating that NVOF-induced neurons appropriately do not co-exhibit multiple neuronal identities. Cultured P2 primary neurons were used as a positive control for immunocytochemistry staining (F, H, J, L, N). Scale bars (E-N) 100 µm.

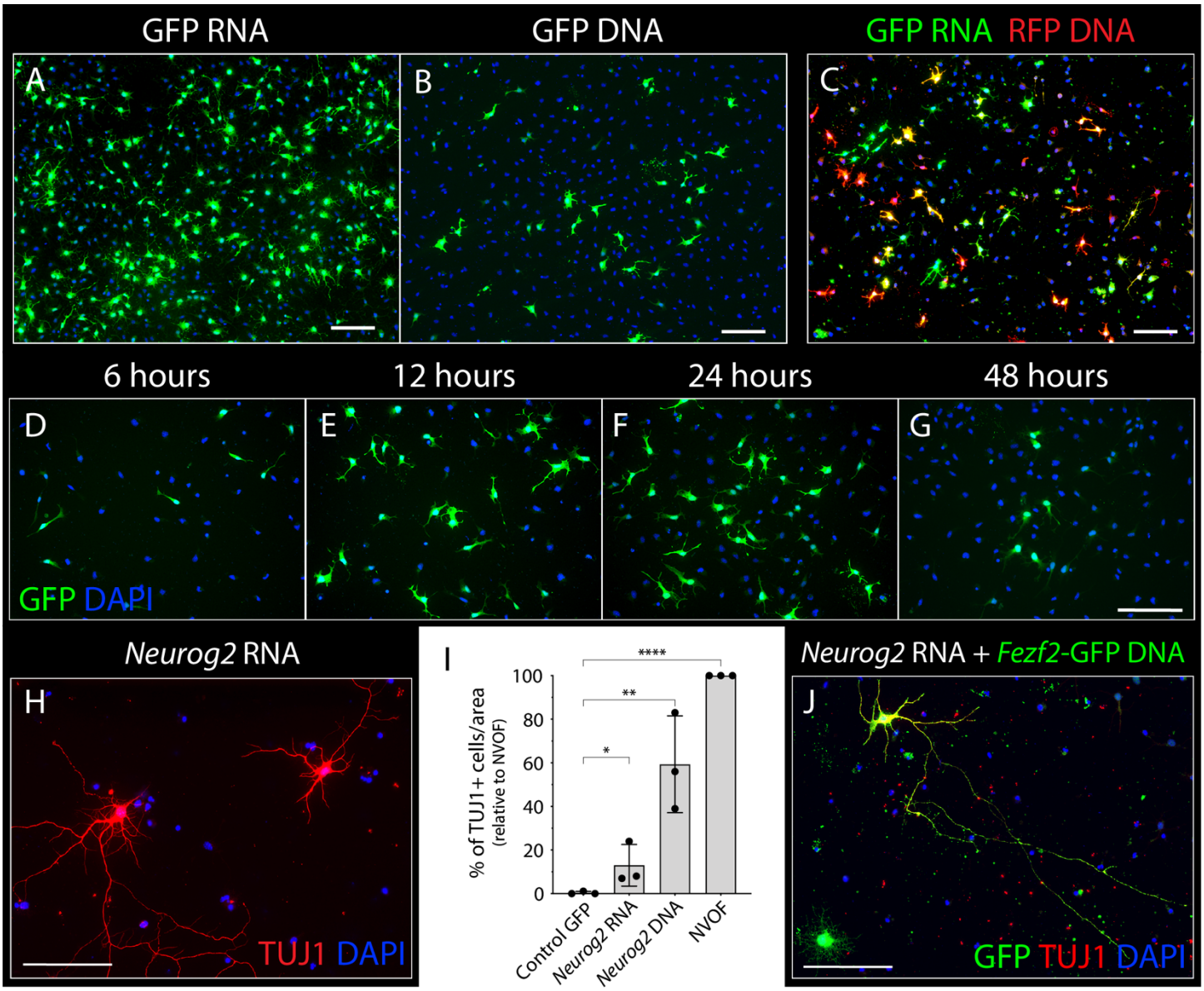

Figure S7. Synthetic mRNA mediates neuronal induction from SOX6+/NG2+ cortical progenitors

(A-B) Cultured progenitors are transfected with GFP RNA at higher efficiency (A) than GFP DNA (B).
(C) Co-transfection of GFP RNA and tdTomato DNA is highly efficient.
(D, G) Time course of gene expression in cultured progenitors transfected with GFP RNA shows that GFP expression begins by 6 hours-post-transfection (D), peaks between 12 and 24 hours (E, F), then declines (G).
(H-I) One pulse of *Neurog2* RNA induces morphologically complex, TUJ1+ neurons from SOX6+/NG2+ cortical progenitors (H), albeit at a lower efficiency than *Neurog2* or NVOF DNA constructs (I). Percentage of TUJ1+, neuron-like cells in cells transfected with GFP control RNA, *Neurog2* RNA, and *Neurog2* DNA relative to the number of TUJ1+ cells after NVOF transfection (I). Error bars show standard deviations. ****$p < 0.0001$, **$p < 0.01$, *$p < 0.05$, t-test. (n=3)
(J) Co-transfection of *Neurog2* RNA and *Fezf2*-GFP DNA induces TUJ1+ neurons from SOX6+/NG2+ progenitors.
Scale bars (A-J) 100 µm.

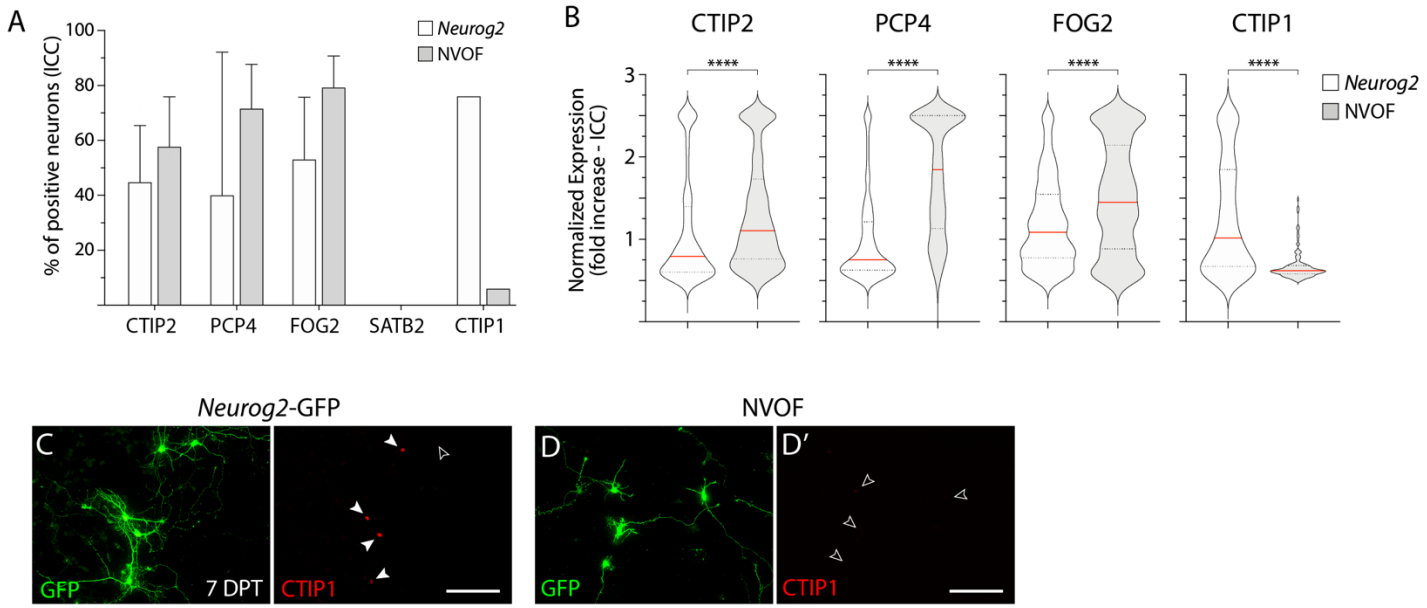

Figure S8. *Neurog2* is not sufficient to induce molecular hallmarks of cortical output neurons

(A) Percentage of *Neurog2*- and NVOF-induced neurons expressing CTIP2, PCP4, FOG2, SATB2, and CTIP1 at 7 DPT.
(B) Quantification of mean fluorescence intensity for CTIP2 (n=~700), PCP4 (n=~450), FOG2 (n=~450), and CTIP1 (n=~150) in *Neurog2*- and NVOF-induced neurons at 7 DPT. Plotted values are mean nuclear intensity of individual neurons normalized to the average intensity of the three lowest-expressing neurons.
(C-D) Representative images of CTIP1 expression by *Neurog2*- (C) and NVOF-induced neurons (D).
Scale bar (C, D) 100 µm. Error bars show standard deviations. ****$p < 0.0001$, t-test in (B).

References

1. Fishell, G., and Rudy, B. (2011). Mechanisms of inhibition within the telencephalon: "where the wild things are". Annu. Rev. Neurosci. *34*, 535–567. 10.1146/annurev-neuro-061010-113717.
2. Greig, L.C., Woodworth, M.B., Galazo, M.J., Padmanabhan, H., and Macklis, J.D. (2013). Molecular logic of neocortical projection neuron specification, development and diversity. Nat. Rev. Neurosci. *14*, 755–769. 10.1038/nrn3586.
3. Harris, K.D., and Shepherd, G.M.G. (2015). The neocortical circuit: themes and variations. Nat. Neurosci. *18*, 170–181. 10.1038/nn.3917.
4. Ramón y Cajal, S. (1995). Histology of the nervous system of man and vertebrates (Oxford University Press).
5. Sugino, K., Hempel, C.M., Miller, M.N., Hattox, A.M., Shapiro, P., Wu, C., Huang, Z.J., and Nelson, S.B. (2006). Molecular taxonomy of major neuronal classes in the adult mouse forebrain. Nat. Neurosci. *9*, 99–107. 10.1038/nn1618.
6. Tasic, B., Yao, Z., Graybuck, L.T., Smith, K.A., Nguyen, T.N., Bertagnolli, D., Goldy, J., Garren, E., Economo, M.N., Viswanathan, S., et al. (2018). Shared and distinct transcriptomic cell types across neocortical areas. Nature *563*, 72–78. 10.1038/s41586-018-0654-5.
7. Veeraraghavan, P., Engmann, A.K., Hatch, J.J., Itoh, Y., Nguyen, D., Addison, T., and Macklis, J.D. (2024). Dynamic subtype- and context-specific subcellular RNA regulation in growth cones of developing neurons of the cerebral cortex. BioRxiv. 10.1101/2023.09.24.559186.
8. Sahni, V., Shnider, S.J., Jabaudon, D., Song, J.H.T., Itoh, Y., Greig, L.C., and Macklis, J.D. (2021). Corticospinal neuron subpopulation-specific developmental genes prospectively indicate mature segmentally specific axon projection targeting. Cell Rep. *37*, 109843. 10.1016/j.celrep.2021.109843.
9. Sahni, V., Itoh, Y., Shnider, S.J., and Macklis, J.D. (2021). Crim1 and Kelch-like 14 exert complementary dual-directional developmental control over segmentally specific corticospinal axon projection targeting. Cell Rep. *37*, 109842. 10.1016/j.celrep.2021.109842.
10. Itoh, Y., Sahni, V., Shnider, S.J., McKee, H., and Macklis, J.D. (2023). Inter-axonal molecular crosstalk via Lumican proteoglycan sculpts murine cervical corticospinal innervation by distinct subpopulations. Cell Rep. *42*, 112182. 10.1016/j.celrep.2023.112182.
11. Sahni, V., Engmann, A., Ozkan, A., and Macklis, J.D. (2020). Motor cortex connections. In Neural circuit and cognitive development (Elsevier), pp. 167–199. 10.1016/B978-0-12-814411-4.00008-1.
12. Saxena, S., and Caroni, P. (2011). Selective neuronal vulnerability in neurodegenerative diseases: from stressor thresholds to degeneration. Neuron *71*, 35–48. 10.1016/j.neuron.2011.06.031.
13. Durak, O., Kim, J.-Y., Tillman, D.E., Itoh, Y., Wettstein, M.R., Greig, L.C., Addison, T.A., and Macklis, J.D. (2022). ASD gene *Bcl11a* regulates subcellular RNA localization, associative circuitry, and social behavior. BioRxiv. 10.1101/2022.10.06.511159.
14. Rosler, K.M., Truffert, A., Hess, C.W., and Magistris, M.R. (2000). Quantification of upper motor neuron loss in amyotrophic lateral sclerosis. Clin Neurophysiol *111*, 2208–2218.
15. Hains, B.C., Black, J.A., and Waxman, S.G. (2003). Primary cortical motor neurons undergo apoptosis after axotomizing spinal cord injury. J. Comp. Neurol. *462*, 328–341. 10.1002/cne.10733.
16. Sances, S., Bruijn, L.I., Chandran, S., Eggan, K., Ho, R., Klim, J.R., Livesey, M.R., Lowry, E., Macklis, J.D., Rushton, D., et al. (2016). Modeling ALS with motor neurons derived from human induced pluripotent stem cells. Nat. Neurosci. *19*, 542–553. 10.1038/nn.4273.
17. Qian, H., Kang, X., Hu, J., Zhang, D., Liang, Z., Meng, F., Zhang, X., Xue, Y., Maimon, R., Dowdy, S.F., et al. (2020). Reversing a model of Parkinson's disease with in situ converted nigral neurons. Nature *582*, 550–556. 10.1038/s41586-020-2388-4.
18. Czupryn, A., Zhou, Y.-D., Chen, X., McNay, D., Anderson, M.P., Flier, J.S., and Macklis, J.D. (2011). Transplanted hypothalamic neurons restore leptin signaling and ameliorate obesity in db/db mice. Science *334*, 1133–1137. 10.1126/science.1209870.
19. Wuttke, T.V., Markopoulos, F., Padmanabhan, H., Wheeler, A.P., Murthy, V.N., and Macklis, J.D. (2018). Developmentally primed cortical neurons maintain fidelity of differentiation and establish appropriate functional connectivity after transplantation. Nat. Neurosci. *21*, 517–529. 10.1038/s41593-018-0098-0.
20. Rietze, R.L., Valcanis, H., Brooker, G.F., Thomas, T., Voss, A.K., and Bartlett, P.F. (2001). Purification of a pluripotent neural stem cell from the adult mouse brain. Nature *412*, 736–739. 10.1038/35089085.
21. Lois, C., and Alvarez-Buylla, A. (1993). Proliferating subventricular zone cells in the adult mammalian forebrain can differentiate into neurons and glia. Proc Natl Acad Sci USA *90*, 2074–2077. 10.1073/pnas.90.5.2074.
22. Kuhn, H.G., Winkler, J., Kempermann, G., Thal, L.J., and Gage, F.H. (1997). Epidermal growth factor and fibroblast growth factor-2 have different effects on neural progenitors in the adult rat brain. J. Neurosci. *17*, 5820–5829. 10.1523/JNEUROSCI.17-15-05820.1997.
23. Reynolds, B.A., and Weiss, S. (1992). Generation of neurons and astrocytes from isolated cells of the adult mammalian central nervous system. Science (New York) *255*, 1707–1710.
24. Kempermann, G., Song, H., and Gage, F.H. (2015). Neurogenesis in the adult hippocampus. Cold Spring Harb. Perspect. Biol. *7*, a018812. 10.1101/cshperspect.a018812.
25. Feliciano, D.M., Bordey, A., and Bonfanti, L. (2015). Noncanonical sites of adult neurogenesis in the mammalian brain. Cold Spring Harb. Perspect. Biol. *7*, a018846. 10.1101/cshperspect.a018846.
26. Magavi, S.S., Leavitt, B.R., and Macklis, J.D. (2000). Induction of neurogenesis in the neocortex of adult mice. Nature *405*, 951–955. 10.1038/35016083.
27. Brill, M.S., Ninkovic, J., Winpenny, E., Hodge, R.D., Ozen, I., Yang, R., Lepier, A., Gascón, S., Erdelyi, F., Szabo, G., et al. (2009). Adult generation of glutamatergic olfactory bulb interneurons. Nat. Neurosci. *12*, 1524–1533. 10.1038/nn.2416.
28. Ohira, K., Furuta, T., Hioki, H., Nakamura, K.C., Kuramoto, E., Tanaka, Y., Funatsu, N., Shimizu, K., Oishi, T., Hayashi, M., et al. (2010). Ischemia-induced neurogenesis of neocortical layer 1 progenitor cells. Nat. Neurosci. *13*, 173–179. 10.1038/nn.2473.
29. Chen, J., Magavi, S.S., and Macklis, J.D. (2004). Neurogenesis of corticospinal motor neurons extending spinal projections in adult mice. Proc Natl Acad Sci U S A *101*, 16357–16362.
30. Michelsen, K.A., Acosta-Verdugo, S., Benoit-Marand, M., Espuny-Camacho, I., Gaspard, N., Saha, B., Gaillard, A., and Vanderhaeghen, P. (2015). Area-specific reestablishment of damaged circuits in the adult cerebral cortex by cortical neurons derived from mouse embryonic stem cells. Neuron *85*, 982–997. 10.1016/j.neuron.2015.02.001.
31. Roessler, R., Smallwood, S.A., Veenvliet, J.V., Pechlivanoglou, P., Peng, S.-P., Chakrabarty, K., Groot-Koerkamp, M.J.A., Pasterkamp, R.J., Wesseling, E., Kelsey, G., et al. (2014). Detailed analysis of the genetic and epigenetic signatures of iPSC-derived mesodiencephalic dopaminergic neurons. Stem Cell Reports *2*, 520–533. 10.1016/j.stemcr.2014.03.001.
32. Treutlein, B., Lee, Q.Y., Camp, J.G., Mall, M., Koh, W., Shariati, S.A.M., Sim, S., Neff, N.F., Skotheim, J.M., Wernig, M., et al. (2016). Dissecting direct reprogramming from fibroblast to neuron using single-cell RNA-seq. Nature *534*, 391–395. 10.1038/nature18323.
33. Cahoy, J.D., Emery, B., Kaushal, A., Foo, L.C., Zamanian, J.L., Christopherson, K.S., Xing, Y., Lubischer, J.L., Krieg, P.A., Krupenko, S.A., et al. (2008). A transcriptome database for astrocytes, neurons, and oligodendrocytes: a new resource for

understanding brain development and function. J. Neurosci. *28*, 264–278. 10.1523/JNEUROSCI.4178-07.2008.

34. Espuny-Camacho, I., Michelsen, K.A., Gall, D., Linaro, D., Hasche, A., Bonnefont, J., Bali, C., Orduz, D., Bilheu, A., Herpoel, A., et al. (2013). Pyramidal neurons derived from human pluripotent stem cells integrate efficiently into mouse brain circuits in vivo. Neuron *77*, 440–456. 10.1016/j.neuron.2012.12.011.
35. Gage, F.H. (2019). Adult neurogenesis in mammals. Science *364*, 827–828. 10.1126/science.aav6885.
36. Bond, A.M., Ming, G.-L., and Song, H. (2015). Adult mammalian neural stem cells and neurogenesis: five decades later. Cell Stem Cell *17*, 385–395. 10.1016/j.stem.2015.09.003.
37. Kempermann, G. (2015). Adult neurogenesis: an evolutionary perspective. Cold Spring Harb. Perspect. Biol. *8*, a018986. 10.1101/cshperspect.a018986.
38. Gascón, S., Murenu, E., Masserdotti, G., Ortega, F., Russo, G.L., Petrik, D., Deshpande, A., Heinrich, C., Karow, M., Robertson, S.P., et al. (2016). Identification and successful negotiation of a metabolic checkpoint in direct neuronal reprogramming. Cell Stem Cell *18*, 396–409. 10.1016/j.stem.2015.12.003.
39. Rivetti di Val Cervo, P., Romanov, R.A., Spigolon, G., Masini, D., Martín-Montañez, E., Toledo, E.M., La Manno, G., Feyder, M., Pifl, C., Ng, Y.-H., et al. (2017). Induction of functional dopamine neurons from human astrocytes in vitro and mouse astrocytes in a Parkinson's disease model. Nat. Biotechnol. *35*, 444–452. 10.1038/nbt.3835.
40. Wu, Z., Parry, M., Hou, X.-Y., Liu, M.-H., Wang, H., Cain, R., Pei, Z.-F., Chen, Y.-C., Guo, Z.-Y., Abhijeet, S., et al. (2020). Gene therapy conversion of striatal astrocytes into GABAergic neurons in mouse models of Huntington's disease. Nat. Commun. *11*, 1105. 10.1038/s41467-020-14855-3.
41. Heinrich, C., Bergami, M., Gascón, S., Lepier, A., Viganò, F., Dimou, L., Sutor, B., Berninger, B., and Götz, M. (2014). Sox2-mediated conversion of NG2 glia into induced neurons in the injured adult cerebral cortex. Stem Cell Reports *3*, 1000–1014. 10.1016/j.stemcr.2014.10.007.
42. Torper, O., Ottosson, D.R., Pereira, M., Lau, S., Cardoso, T., Grealish, S., and Parmar, M. (2015). In Vivo Reprogramming of Striatal NG2 Glia into Functional Neurons that Integrate into Local Host Circuitry. Cell Rep. *12*, 474–481. 10.1016/j.celrep.2015.06.040.
43. Grande, A., Sumiyoshi, K., López-Juárez, A., Howard, J., Sakthivel, B., Aronow, B., Campbell, K., and Nakafuku, M. (2013). Environmental impact on direct neuronal reprogramming in vivo in the adult brain. Nat. Commun. *4*, 2373. 10.1038/ncomms3373.
44. Niu, W., Zang, T., Zou, Y., Fang, S., Smith, D.K., Bachoo, R., and Zhang, C.-L. (2013). In vivo reprogramming of astrocytes to neuroblasts in the adult brain. Nat. Cell Biol. *15*, 1164–1175. 10.1038/ncb2843.
45. Heinrich, C., Blum, R., Gascón, S., Masserdotti, G., Tripathi, P., Sánchez, R., Tiedt, S., Schroeder, T., Götz, M., and Berninger, B. (2010). Directing astroglia from the cerebral cortex into subtype specific functional neurons. PLoS Biol. *8*, e1000373. 10.1371/journal.pbio.1000373.
46. Mattugini, N., Bocchi, R., Scheuss, V., Russo, G.L., Torper, O., Lao, C.L., and Götz, M. (2019). Inducing Different Neuronal Subtypes from Astrocytes in the Injured Mouse Cerebral Cortex. Neuron *103*, 1086-1095.e5. 10.1016/j.neuron.2019.08.009.
47. Arlotta, P., Molyneaux, B.J., Chen, J., Inoue, J., Kominami, R., and Macklis, J.D. (2005). Neuronal subtype-specific genes that control corticospinal motor neuron development in vivo. Neuron *45*, 207–221. 10.1016/j.neuron.2004.12.036.
48. Lodato, S., and Arlotta, P. (2015). Generating neuronal diversity in the mammalian cerebral cortex. Annu. Rev. Cell Dev. Biol. *31*, 699–720. 10.1146/annurev-cellbio-100814-125353.
49. Ozkan, A., MacDonald, J.L., Fame, R.M., Itoh, Y., Peter, M., Durak, O., and Macklis, J.D. (2020). Specification of cortical projection neurons. In Patterning and cell type specification in the developing CNS and PNS (Elsevier), pp. 427–459. 10.1016/B978-0-12-814405-3.00019-9.
50. Shibata, M., Gulden, F.O., and Sestan, N. (2015). From trans to cis: transcriptional regulatory networks in neocortical development. Trends Genet. *31*, 77–87. 10.1016/j.tig.2014.12.004.
51. Nord, A.S., Pattabiraman, K., Visel, A., and Rubenstein, J.L.R. (2015). Genomic perspectives of transcriptional regulation in forebrain development. Neuron *85*, 27–47. 10.1016/j.neuron.2014.11.011.
52. Taverna, E., Götz, M., and Huttner, W.B. (2014). The cell biology of neurogenesis: toward an understanding of the development and evolution of the neocortex. Annu. Rev. Cell Dev. Biol. *30*, 465–502. 10.1146/annurev-cellbio-101011-155801.
53. Srinivasan, K., Leone, D.P., Bateson, R.K., Dobreva, G., Kohwi, Y., Kohwi-Shigematsu, T., Grosschedl, R., and McConnell, S.K. (2012). A network of genetic repression and derepression specifies projection fates in the developing neocortex. Proc Natl Acad Sci USA *109*, 19071–19078. 10.1073/pnas.1216793109.
54. Lui, J.H., Hansen, D.V., and Kriegstein, A.R. (2011). Development and evolution of the human neocortex. Cell *146*, 18–36. 10.1016/j.cell.2011.06.030.
55. O'Leary, D.D.M., Chou, S.-J., and Sahara, S. (2007). Area patterning of the mammalian cortex. Neuron *56*, 252–269. 10.1016/j.neuron.2007.10.010.
56. Greig, L.C., Woodworth, M.B., Greppi, C., and Macklis, J.D. (2016). Ctip1 controls acquisition of sensory area identity and establishment of sensory input fields in the developing neocortex. Neuron *90*, 261–277. 10.1016/j.neuron.2016.03.008.
57. Woodworth, M.B., Greig, L.C., Liu, K.X., Ippolito, G.C., Tucker, H.O., and Macklis, J.D. (2016). Ctip1 Regulates the Balance between Specification of Distinct Projection Neuron Subtypes in Deep Cortical Layers. Cell Rep. *15*, 999–1012. 10.1016/j.celrep.2016.03.064.
58. Galazo, M.J., Emsley, J.G., and Macklis, J.D. (2016). Corticothalamic Projection Neuron Development beyond Subtype Specification: Fog2 and Intersectional Controls Regulate Intraclass Neuronal Diversity. Neuron *91*, 90–106. 10.1016/j.neuron.2016.05.024.
59. Galazo, M.J., Sweetser, D.A., and Macklis, J.D. (2023). Tle4 controls both developmental acquisition and early post-natal maturation of corticothalamic projection neuron identity. Cell Rep. *42*, 112957. 10.1016/j.celrep.2023.112957.
60. Azim, E., Jabaudon, D., Fame, R.M., and Macklis, J.D. (2009). SOX6 controls dorsal-ventral progenitor parcellation and interneuron diversity during development of the neocortex. Nat Neurosci *12*, 1238–1247.
61. Burns, K.A., Murphy, B., Danzer, S.C., and Kuan, C.-Y. (2009). Developmental and post-injury cortical gliogenesis: a genetic fate-mapping study with Nestin-CreER mice. Glia *57*, 1115–1129. 10.1002/glia.20835.
62. Elsherbiny, A., and Dobreva, G. (2021). Epigenetic memory of cell fate commitment. Curr. Opin. Cell Biol. *69*, 80–87. 10.1016/j.ceb.2020.12.014.
63. Zhang, Y., Chen, K., Sloan, S.A., Bennett, M.L., Scholze, A.R., O'Keeffe, S., Phatnani, H.P., Guarnieri, P., Caneda, C., Ruderisch, N., et al. (2014). An RNA-sequencing transcriptome and splicing database of glia, neurons, and vascular cells of the cerebral cortex. J. Neurosci. *34*, 11929–11947. 10.1523/JNEUROSCI.1860-14.2014.
64. Hevner, R.F. (2006). From radial glia to pyramidal-projection neuron: transcription factor cascades in cerebral cortex development. Mol. Neurobiol. *33*, 33–50. 10.1385/MN:33:1:033.
65. Woodworth, M.B., Greig, L.C., Kriegstein, A.R., and Macklis, J.D. (2012). SnapShot: cortical development. Cell *151*, 918-918.e1. 10.1016/j.cell.2012.10.004.

66. Zhu, X., Bergles, D.E., and Nishiyama, A. (2008). NG2 cells generate both oligodendrocytes and gray matter astrocytes. Development *135*, 145–157. 10.1242/dev.004895.

67. Lyssiotis, C.A., Walker, J., Wu, C., Kondo, T., Schultz, P.G., and Wu, X. (2007). Inhibition of histone deacetylase activity induces developmental plasticity in oligodendrocyte precursor cells. Proc Natl Acad Sci USA *104*, 14982–14987. 10.1073/pnas.0707044104.

68. Hughes, E.G., Kang, S.H., Fukaya, M., and Bergles, D.E. (2013). Oligodendrocyte progenitors balance growth with self-repulsion to achieve homeostasis in the adult brain. Nat. Neurosci. *16*, 668–676. 10.1038/nn.3390.

69. Baroti, T., Zimmermann, Y., Schillinger, A., Liu, L., Lommes, P., Wegner, M., and Stolt, C.C. (2016). Transcription factors Sox5 and Sox6 exert direct and indirect influences on oligodendroglial migration in spinal cord and forebrain. Glia *64*, 122–138. 10.1002/glia.22919.

70. Stolt, C.C., Schlierf, A., Lommes, P., Hillgärtner, S., Werner, T., Kosian, T., Sock, E., Kessaris, N., Richardson, W.D., Lefebvre, V., et al. (2006). SoxD proteins influence multiple stages of oligodendrocyte development and modulate SoxE protein function. Dev. Cell *11*, 697–709. 10.1016/j.devcel.2006.08.011.

71. Ozerdem, U., Grako, K.A., Dahlin-Huppe, K., Monosov, E., and Stallcup, W.B. (2001). NG2 proteoglycan is expressed exclusively by mural cells during vascular morphogenesis. Dev. Dyn. *222*, 218–227. 10.1002/dvdy.1200.

72. Tang, W., Ehrlich, I., Wolff, S.B.E., Michalski, A.-M., Wölfl, S., Hasan, M.T., Lüthi, A., and Sprengel, R. (2009). Faithful expression of multiple proteins via 2A-peptide self-processing: a versatile and reliable method for manipulating brain circuits. J. Neurosci. *29*, 8621–8629. 10.1523/JNEUROSCI.0359-09.2009.

73. Schuurmans, C., Armant, O., Nieto, M., Stenman, J.M., Britz, O., Klenin, N., Brown, C., Langevin, L.-M., Seibt, J., Tang, H., et al. (2004). Sequential phases of cortical specification involve Neurogenin-dependent and -independent pathways. EMBO J. *23*, 2892–2902. 10.1038/sj.emboj.7600278.

74. Mattar, P., Langevin, L.M., Markham, K., Klenin, N., Shivji, S., Zinyk, D., and Schuurmans, C. (2008). Basic helix-loop-helix transcription factors cooperate to specify a cortical projection neuron identity. Mol. Cell. Biol. *28*, 1456–1469. 10.1128/MCB.01510-07.

75. Zhang, Y., Pak, C., Han, Y., Ahlenius, H., Zhang, Z., Chanda, S., Marro, S., Patzke, C., Acuna, C., Covy, J., et al. (2013). Rapid single-step induction of functional neurons from human pluripotent stem cells. Neuron *78*, 785–798. 10.1016/j.neuron.2013.05.029.

76. Hulme, A.J., Maksour, S., St-Clair Glover, M., Miellet, S., and Dottori, M. (2022). Making neurons, made easy: The use of Neurogenin-2 in neuronal differentiation. Stem Cell Reports *17*, 14–34. 10.1016/j.stemcr.2021.11.015.

77. Mizuguchi, R., Sugimori, M., Takebayashi, H., Kosako, H., Nagao, M., Yoshida, S., Nabeshima, Y., Shimamura, K., and Nakafuku, M. (2001). Combinatorial roles of olig2 and neurogenin2 in the coordinated induction of pan-neuronal and subtype-specific properties of motoneurons. Neuron *31*, 757–771. 10.1016/s0896-6273(01)00413-5.

78. Novitch, B.G., Chen, A.I., and Jessell, T.M. (2001). Coordinate regulation of motor neuron subtype identity and pan-neuronal properties by the bHLH repressor Olig2. Neuron *31*, 773–789. 10.1016/s0896-6273(01)00407-x.

79. Zhou, Q., Choi, G., and Anderson, D.J. (2001). The bHLH transcription factor Olig2 promotes oligodendrocyte differentiation in collaboration with Nkx2.2. Neuron *31*, 791–807. 10.1016/s0896-6273(01)00414-7.

80. Li, H., and Richardson, W.D. (2016). Evolution of the CNS myelin gene regulatory program. Brain Res. *1641*, 111–121. 10.1016/j.brainres.2015.10.013.

81. Lee, S.-K., Lee, B., Ruiz, E.C., and Pfaff, S.L. (2005). Olig2 and Ngn2 function in opposition to modulate gene expression in motor neuron progenitor cells. Genes Dev. *19*, 282–294. 10.1101/gad.1257105.

82. Liu, W., Zhou, H., Liu, L., Zhao, C., Deng, Y., Chen, L., Wu, L., Mandrycky, N., McNabb, C.T., Peng, Y., et al. (2015). Disruption of neurogenesis and cortical development in transgenic mice misexpressing Olig2, a gene in the Down syndrome critical region. Neurobiol. Dis. *77*, 106–116. 10.1016/j.nbd.2015.02.021.

83. Buffo, A., Vosko, M.R., Ertürk, D., Hamann, G.F., Jucker, M., Rowitch, D., and Götz, M. (2005). Expression pattern of the transcription factor Olig2 in response to brain injuries: implications for neuronal repair. Proc Natl Acad Sci USA *102*, 18183–18188. 10.1073/pnas.0506535102.

84. Kronenberg, G., Gertz, K., Cheung, G., Buffo, A., Kettenmann, H., Götz, M., and Endres, M. (2010). Modulation of fate determinants Olig2 and Pax6 in resident glia evokes spiking neuroblasts in a model of mild brain ischemia. Stroke *41*, 2944–2949. 10.1161/STROKEAHA.110.583039.

85. Molyneaux, B.J., Arlotta, P., Hirata, T., Hibi, M., and Macklis, J.D. (2005). Fezl is required for the birth and specification of corticospinal motor neurons. Neuron *47*, 817–831. 10.1016/j.neuron.2005.08.030.

86. Rouaux, C., and Arlotta, P. (2010). Fezf2 directs the differentiation of corticofugal neurons from striatal progenitors in vivo. Nat. Neurosci. *13*, 1345–1347. 10.1038/nn.2658.

87. De la Rossa, A., Bellone, C., Golding, B., Vitali, I., Moss, J., Toni, N., Lüscher, C., and Jabaudon, D. (2013). In vivo reprogramming of circuit connectivity in postmitotic neocortical neurons. Nat. Neurosci. *16*, 193–200. 10.1038/nn.3299.

88. Funahashi, Y., Watanabe, T., and Kaibuchi, K. (2020). Advances in defining signaling networks for the establishment of neuronal polarity. Curr. Opin. Cell Biol. *63*, 76–87. 10.1016/j.ceb.2019.12.009.

89. Lin, H.-C., He, Z., Ebert, S., Schörnig, M., Santel, M., Nikolova, M.T., Weigert, A., Hevers, W., Kasri, N.N., Taverna, E., et al. (2021). NGN2 induces diverse neuron types from human pluripotency. Stem Cell Reports *16*, 2118–2127. 10.1016/j.stemcr.2021.07.006.

90. Kempf, J., Knelles, K., Hersbach, B.A., Petrik, D., Riedemann, T., Bednarova, V., Janjic, A., Simon-Ebert, T., Enard, W., Smialowski, P., et al. (2021). Heterogeneity of neurons reprogrammed from spinal cord astrocytes by the proneural factors Ascl1 and Neurogenin2. Cell Rep. *36*, 109409. 10.1016/j.celrep.2021.109409.

91. Chouchane, M., Melo de Farias, A.R., Moura, D.M. de S., Hilscher, M.M., Schroeder, T., Leão, R.N., and Costa, M.R. (2017). Lineage Reprogramming of Astroglial Cells from Different Origins into Distinct Neuronal Subtypes. Stem Cell Reports *9*, 162–176. 10.1016/j.stemcr.2017.05.009.

92. Sheta, R., Teixeira, M., Idi, W., Pierre, M., de Rus Jacquet, A., Emond, V., Zorca, C.E., Vanderperre, B., Durcan, T.M., Fon, E.A., et al. (2022). Combining NGN2 programming and dopaminergic patterning for a rapid and efficient generation of hiPSC-derived midbrain neurons. Sci. Rep. *12*, 17176. 10.1038/s41598-022-22158-4.

93. Ang, C.E., Olmos, V.H., Vodehnal, K., Zhou, B., Lee, Q.Y., Sinha, R., Narayanaswamy, A., Mall, M., Chesnov, K., Dominicus, C.S., et al. (2024). Generation of human excitatory forebrain neurons by cooperative binding of proneural NGN2 and homeobox factor EMX1. Proc Natl Acad Sci USA *121*, e2308401121. 10.1073/pnas.2308401121.

94. Kaech, S., and Banker, G. (2006). Culturing hippocampal neurons. Nat. Protoc. *1*, 2406–2415. 10.1038/nprot.2006.356.

95. Pfrieger, F.W., and Barres, B.A. (1997). Synaptic efficacy enhanced by glial cells in vitro. Science *277*, 1684–1687. 10.1126/science.277.5332.1684.

96. Cai, L., Morrow, E.M., and Cepko, C.L. (2000). Misexpression of basic helix-loop-helix genes in the murine cerebral cortex affects

cell fate choices and neuronal survival. Development *127*, 3021–3030. 10.1242/dev.127.14.3021.

97. Sahin, U., Karikó, K., and Türeci, Ö. (2014). mRNA-based therapeutics--developing a new class of drugs. Nat. Rev. Drug Discov. *13*, 759–780. 10.1038/nrd4278.

98. Warren, L., Manos, P.D., Ahfeldt, T., Loh, Y.-H., Li, H., Lau, F., Ebina, W., Mandal, P.K., Smith, Z.D., Meissner, A., et al. (2010). Highly efficient reprogramming to pluripotency and directed differentiation of human cells with synthetic modified mRNA. Cell Stem Cell *7*, 618–630. 10.1016/j.stem.2010.08.012.

99. Hisaoka, T., Nakamura, Y., Senba, E., and Morikawa, Y. (2010). The forkhead transcription factors, Foxp1 and Foxp2, identify different subpopulations of projection neurons in the mouse cerebral cortex. Neuroscience *166*, 551–563. 10.1016/j.neuroscience.2009.12.055.

100. Sadegh, C., and Macklis, J.D. (2014). Established monolayer differentiation of mouse embryonic stem cells generates heterogeneous neocortical-like neurons stalled at a stage equivalent to midcorticogenesis. J. Comp. Neurol. *522*, 2691–2706. 10.1002/cne.23576.

101. Molyneaux, B.J., Goff, L.A., Brettler, A.C., Chen, H.-H., Hrvatin, S., Rinn, J.L., and Arlotta, P. (2015). DeCoN: genome-wide analysis of in vivo transcriptional dynamics during pyramidal neuron fate selection in neocortex. Neuron *85*, 275–288. 10.1016/j.neuron.2014.12.024.

102. Lodato, S., Molyneaux, B.J., Zuccaro, E., Goff, L.A., Chen, H.-H., Yuan, W., Meleski, A., Takahashi, E., Mahony, S., Rinn, J.L., et al. (2014). Gene co-regulation by Fezf2 selects neurotransmitter identity and connectivity of corticospinal neurons. Nat. Neurosci. *17*, 1046–1054. 10.1038/nn.3757.

103. Alcamo, E.A., Chirivella, L., Dautzenberg, M., Dobreva, G., Fariñas, I., Grosschedl, R., and McConnell, S.K. (2008). Satb2 regulates callosal projection neuron identity in the developing cerebral cortex. Neuron *57*, 364–377. 10.1016/j.neuron.2007.12.012.

104. Nishikimi, M., Oishi, K., Tabata, H., Torii, K., and Nakajima, K. (2011). Segregation and pathfinding of callosal axons through EphA3 signaling. J. Neurosci. *31*, 16251–16260. 10.1523/JNEUROSCI.3303-11.2011.

105. Ozdinler, P.H., and Macklis, J.D. (2006). IGF-I specifically enhances axon outgrowth of corticospinal motor neurons. Nat. Neurosci. *9*, 1371–1381. 10.1038/nn1789.

106. Britz, O., Mattar, P., Nguyen, L., Langevin, L.-M., Zimmer, C., Alam, S., Guillemot, F., and Schuurmans, C. (2006). A role for proneural genes in the maturation of cortical progenitor cells. Cereb. Cortex *16 Suppl 1*, i138-51. 10.1093/cercor/bhj168.

107. Hand, R., and Polleux, F. (2011). Neurogenin2 regulates the initial axon guidance of cortical pyramidal neurons projecting medially to the corpus callosum. Neural Dev. *6*, 30. 10.1186/1749-8104-6-30.

108. Dennis, D.J., Wilkinson, G., Li, S., Dixit, R., Adnani, L., Balakrishnan, A., Han, S., Kovach, C., Gruenig, N., Kurrasch, D.M., et al. (2017). Neurog2 and Ascl1 together regulate a postmitotic derepression circuit to govern laminar fate specification in the murine neocortex. Proc Natl Acad Sci USA *114*, E4934–E4943. 10.1073/pnas.1701495114.

109. Chen, M., Maimaitili, M., Habekost, M., Gill, K.P., Mermet-Joret, N., Nabavi, S., Febbraro, F., and Denham, M. (2020). Rapid generation of regionally specified CNS neurons by sequential patterning and conversion of human induced pluripotent stem cells. Stem Cell Res. *48*, 101945. 10.1016/j.scr.2020.101945.

110. Rosa, F., Dhingra, A., Uysal, B., Mendis, G.D.C., Loeffler, H., Elsen, G., Mueller, S., Schwarz, N., Castillo-Lizardo, M., Cuddy, C., et al. (2020). In Vitro Differentiated Human Stem Cell-Derived Neurons Reproduce Synaptic Synchronicity Arising during Neurodevelopment. Stem Cell Reports *15*, 22–37. 10.1016/j.stemcr.2020.05.015.

111. McKenna, W.L., Betancourt, J., Larkin, K.A., Abrams, B., Guo, C., Rubenstein, J.L.R., and Chen, B. (2011). Tbr1 and Fezf2 regulate alternate corticofugal neuronal identities during neocortical development. J. Neurosci. *31*, 549–564. 10.1523/JNEUROSCI.4131-10.2011.

112. Han, W., Kwan, K.Y., Shim, S., Lam, M.M.S., Shin, Y., Xu, X., Zhu, Y., Li, M., and Sestan, N. (2011). TBR1 directly represses Fezf2 to control the laminar origin and development of the corticospinal tract. Proc Natl Acad Sci USA *108*, 3041–3046. 10.1073/pnas.1016723108.

113. Lai, T., Jabaudon, D., Molyneaux, B.J., Azim, E., Arlotta, P., Menezes, J.R.L., and Macklis, J.D. (2008). SOX5 controls the sequential generation of distinct corticofugal neuron subtypes. Neuron *57*, 232–247. 10.1016/j.neuron.2007.12.023.

114. Hirata, T., Suda, Y., Nakao, K., Narimatsu, M., Hirano, T., and Hibi, M. (2004). Zinc finger gene fez-like functions in the formation of subplate neurons and thalamocortical axons. Dev. Dyn. *230*, 546–556. 10.1002/dvdy.20068.

115. Azim, E., Shnider, S.J., Cederquist, G.Y., Sohur, U.S., and Macklis, J.D. (2009). Lmo4 and Clim1 progressively delineate cortical projection neuron subtypes during development. Cereb. Cortex *19 Suppl 1*, i62-9. 10.1093/cercor/bhp030.

116. Cederquist, G.Y., Azim, E., Shnider, S.J., Padmanabhan, H., and Macklis, J.D. (2013). Lmo4 establishes rostral motor cortex projection neuron subtype diversity. J. Neurosci. *33*, 6321–6332. 10.1523/JNEUROSCI.5140-12.2013.

117. Shimojo, H., Ohtsuka, T., and Kageyama, R. (2011). Dynamic expression of notch signaling genes in neural stem/progenitor cells. Front. Neurosci. *5*, 78. 10.3389/fnins.2011.00078.

118. Kovach, C., Dixit, R., Li, S., Mattar, P., Wilkinson, G., Elsen, G.E., Kurrasch, D.M., Hevner, R.F., and Schuurmans, C. (2013). Neurog2 simultaneously activates and represses alternative gene expression programs in the developing neocortex. Cereb. Cortex *23*, 1884–1900. 10.1093/cercor/bhs176.

119. Polo, J.M., Liu, S., Figueroa, M.E., Kulalert, W., Eminli, S., Tan, K.Y., Apostolou, E., Stadtfeld, M., Li, Y., Shioda, T., et al. (2010). Cell type of origin influences the molecular and functional properties of mouse induced pluripotent stem cells. Nat. Biotechnol. *28*, 848–855. 10.1038/nbt.1667.

120. Beagan, J.A., Gilgenast, T.G., Kim, J., Plona, Z., Norton, H.K., Hu, G., Hsu, S.C., Shields, E.J., Lyu, X., Apostolou, E., et al. (2016). Local Genome Topology Can Exhibit an Incompletely Rewired 3D-Folding State during Somatic Cell Reprogramming. Cell Stem Cell *18*, 611–624. 10.1016/j.stem.2016.04.004.

121. Krijger, P.H.L., Di Stefano, B., de Wit, E., Limone, F., van Oevelen, C., de Laat, W., and Graf, T. (2016). Cell-of-Origin-Specific 3D Genome Structure Acquired during Somatic Cell Reprogramming. Cell Stem Cell *18*, 597–610. 10.1016/j.stem.2016.01.007.

122. Ninkovic, J., and Götz, M. (2015). How to make neurons--thoughts on the molecular logic of neurogenesis in the central nervous system. Cell Tissue Res. *359*, 5–16. 10.1007/s00441-014-2048-9.

123. Dawson, M.R.L., Polito, A., Levine, J.M., and Reynolds, R. (2003). NG2-expressing glial progenitor cells: an abundant and widespread population of cycling cells in the adult rat CNS. Mol. Cell. Neurosci. *24*, 476–488. 10.1016/s1044-7431(03)00210-0.

124. Huang, W., Bhaduri, A., Velmeshev, D., Wang, S., Wang, L., Rottkamp, C.A., Alvarez-Buylla, A., Rowitch, D.H., and Kriegstein, A.R. (2020). Origins and proliferative states of human oligodendrocyte precursor cells. Cell *182*, 594-608.e11. 10.1016/j.cell.2020.06.027.

125. Viganò, F., and Dimou, L. (2016). The heterogeneous nature of NG2-glia. Brain Res. *1638*, 129–137. 10.1016/j.brainres.2015.09.012.

126. Chamling, X., Kallman, A., Fang, W., Berlinicke, C.A., Mertz, J.L., Devkota, P., Pantoja, I.E.M., Smith, M.D., Ji, Z., Chang, C., et al. (2021). Single-cell transcriptomic reveals molecular diversity and developmental heterogeneity of human stem cell-derived

oligodendrocyte lineage cells. Nat. Commun. *12*, 652. 10.1038/s41467-021-20892-3.

127. Fang, L.-P., Liu, Q., Meyer, E., Welle, A., Huang, W., Scheller, A., Kirchhoff, F., and Bai, X. (2022). A subset of OPCs do not express Olig2 during development which can be increased in the adult by brain injuries and complex motor learning. Glia. 10.1002/glia.24284.

128. Marisca, R., Hoche, T., Agirre, E., Hoodless, L.J., Barkey, W., Auer, F., Castelo-Branco, G., and Czopka, T. (2020). Functionally distinct subgroups of oligodendrocyte precursor cells integrate neural activity and execute myelin formation. Nat. Neurosci. *23*, 363–374. 10.1038/s41593-019-0581-2.

129. Spitzer, S.O., Sitnikov, S., Kamen, Y., Evans, K.A., Kronenberg-Versteeg, D., Dietmann, S., de Faria, O., Agathou, S., and Káradóttir, R.T. (2019). Oligodendrocyte Progenitor Cells Become Regionally Diverse and Heterogeneous with Age. Neuron *101*, 459-471.e5. 10.1016/j.neuron.2018.12.020.

130. Sánchez-González, R., Bribián, A., and López-Mascaraque, L. (2020). Cell fate potential of NG2 progenitors. Sci. Rep. *10*, 9876. 10.1038/s41598-020-66753-9.

131. Janeckova, L., Knotek, T., Kriska, J., Hermanova, Z., Kirdajova, D., Kubovciak, J., Berkova, L., Tureckova, J., Camacho Garcia, S., Galuskova, K., et al. (2023). Astrocyte-like subpopulation of NG2 glia in the adult mouse cortex exhibits characteristics of neural progenitor cells. Glia. 10.1002/glia.24471.

132. Kirdajova, D., Valihrach, L., Valny, M., Kriska, J., Krocianova, D., Benesova, S., Abaffy, P., Zucha, D., Klassen, R., Kolenicova, D., et al. (2021). Transient astrocyte-like NG2 glia subpopulation emerges solely following permanent brain ischemia. Glia. 10.1002/glia.24064.

133. Tsoa, R.W., Coskun, V., Ho, C.K., de Vellis, J., and Sun, Y.E. (2014). Spatiotemporally different origins of NG2 progenitors produce cortical interneurons versus glia in the mammalian forebrain. Proc Natl Acad Sci USA *111*, 7444–7449. 10.1073/pnas.1400422111.

134. Hilscher, M.M., Langseth, C.M., Kukanja, P., Yokota, C., Nilsson, M., and Castelo-Branco, G. (2022). Spatial and temporal heterogeneity in the lineage progression of fine oligodendrocyte subtypes. BMC Biol. *20*, 122. 10.1186/s12915-022-01325-z.

135. Floriddia, E.M., Lourenço, T., Zhang, S., van Bruggen, D., Hilscher, M.M., Kukanja, P., Gonçalves Dos Santos, J.P., Altınkök, M., Yokota, C., Llorens-Bobadilla, E., et al. (2020). Distinct oligodendrocyte populations have spatial preference and different responses to spinal cord injury. Nat. Commun. *11*, 5860. 10.1038/s41467-020-19453-x.

136. Zhu, X., Hill, R.A., and Nishiyama, A. (2008). NG2 cells generate oligodendrocytes and gray matter astrocytes in the spinal cord. Neuron Glia Biol. *4*, 19–26. 10.1017/S1740925X09000015.

137. Rivers, L.E., Young, K.M., Rizzi, M., Jamen, F., Psachoulia, K., Wade, A., Kessaris, N., and Richardson, W.D. (2008). PDGFRA/NG2 glia generate myelinating oligodendrocytes and piriform projection neurons in adult mice. Nat. Neurosci. *11*, 1392–1401. 10.1038/nn.2220.

138. Guo, F., Maeda, Y., Ma, J., Xu, J., Horiuchi, M., Miers, L., Vaccarino, F., and Pleasure, D. (2010). Pyramidal neurons are generated from oligodendroglial progenitor cells in adult piriform cortex. J. Neurosci. *30*, 12036–12049. 10.1523/JNEUROSCI.1360-10.2010.

139. Liu, R., Jia, Y., Guo, P., Jiang, W., Bai, R., and Liu, C. (2021). In Vivo Clonal Analysis Reveals Development Heterogeneity of Oligodendrocyte Precursor Cells Derived from Distinct Germinal Zones. Adv Sci (Weinh) *8*, e2102274. 10.1002/advs.202102274.

140. Kessaris, N., Fogarty, M., Iannarelli, P., Grist, M., Wegner, M., and Richardson, W.D. (2006). Competing waves of oligodendrocytes in the forebrain and postnatal elimination of an embryonic lineage. Nat. Neurosci. *9*, 173–179. 10.1038/nn1620.

141. Tripathi, R.B., Clarke, L.E., Burzomato, V., Kessaris, N., Anderson, P.N., Attwell, D., and Richardson, W.D. (2011). Dorsally and ventrally derived oligodendrocytes have similar electrical properties but myelinate preferred tracts. J. Neurosci. *31*, 6809–6819. 10.1523/JNEUROSCI.6474-10.2011.

142. Trotter, J., Karram, K., and Nishiyama, A. (2010). NG2 cells: Properties, progeny and origin. Brain Res. Rev. *63*, 72–82. 10.1016/j.brainresrev.2009.12.006.

143. Autar, K., Guo, X., Rumsey, J.W., Long, C.J., Akanda, N., Jackson, M., Narasimhan, N.S., Caneus, J., Morgan, D., and Hickman, J.J. (2022). A functional hiPSC-cortical neuron differentiation and maturation model and its application to neurological disorders. Stem Cell Reports *17*, 96–109. 10.1016/j.stemcr.2021.11.009.

144. Cao, S.-Y., Hu, Y., Chen, C., Yuan, F., Xu, M., Li, Q., Fang, K.-H., Chen, Y., and Liu, Y. (2017). Enhanced derivation of human pluripotent stem cell-derived cortical glutamatergic neurons by a small molecule. Sci. Rep. *7*, 3282. 10.1038/s41598-017-03519-w.

145. Miskinyte, G., Devaraju, K., Grønning Hansen, M., Monni, E., Tornero, D., Woods, N.B., Bengzon, J., Ahlenius, H., Lindvall, O., and Kokaia, Z. (2017). Direct conversion of human fibroblasts to functional excitatory cortical neurons integrating into human neural networks. Stem Cell Res. Ther. *8*, 207. 10.1186/s13287-017-0658-3.

146. Kim, K., Doi, A., Wen, B., Ng, K., Zhao, R., Cahan, P., Kim, J., Aryee, M.J., Ji, H., Ehrlich, L.I.R., et al. (2010). Epigenetic memory in induced pluripotent stem cells. Nature *467*, 285–290. 10.1038/nature09342.

147. Smits, P., Li, P., Mandel, J., Zhang, Z., Deng, J.M., Behringer, R.R., de Crombrugghe, B., and Lefebvre, V. (2001). The transcription factors L-Sox5 and Sox6 are essential for cartilage formation. Dev. Cell *1*, 277–290. 10.1016/s1534-5807(01)00003-x.

148. Donnelly, M.L.L., Luke, G., Mehrotra, A., Li, X., Hughes, L.E., Gani, D., and Ryan, M.D. (2001). Analysis of the aphthovirus 2A/2B polyprotein "cleavage" mechanism indicates not a proteolytic reaction, but a novel translational effect: a putative ribosomal "skip". J. Gen. Virol. *82*, 1013–1025. 10.1099/0022-1317-82-5-1013.

149. Szymczak, A.L., Workman, C.J., Wang, Y., Vignali, K.M., Dilioglou, S., Vanin, E.F., and Vignali, D.A.A. (2004). Correction of multi-gene deficiency in vivo using a single "self-cleaving" 2A peptide-based retroviral vector. Nat. Biotechnol. *22*, 589–594. 10.1038/nbt957.

150. Mandal, P.K., and Rossi, D.J. (2013). Reprogramming human fibroblasts to pluripotency using modified mRNA. Nat. Protoc. *8*, 568–582. 10.1038/nprot.2013.019.

151. Catapano, L.A., Arnold, M.W., Perez, F.A., and Macklis, J.D. (2001). Specific neurotrophic factors support the survival of cortical projection neurons at distinct stages of development. J. Neurosci. *21*, 8863–8872. 10.1523/JNEUROSCI.21-22-08863.2001.

152. Najm, F.J., Lager, A.M., Zaremba, A., Wyatt, K., Caprariello, A.V., Factor, D.C., Karl, R.T., Maeda, T., Miller, R.H., and Tesar, P.J. (2013). Transcription factor-mediated reprogramming of fibroblasts to expandable, myelinogenic oligodendrocyte progenitor cells. Nat. Biotechnol. *31*, 426–433. 10.1038/nbt.2561.

153. Heinrich, C., Gascón, S., Masserdotti, G., Lepier, A., Sanchez, R., Simon-Ebert, T., Schroeder, T., Götz, M., and Berninger, B. (2011). Generation of subtype-specific neurons from postnatal astroglia of the mouse cerebral cortex. Nat. Protoc. *6*, 214–228. 10.1038/nprot.2010.188.

154. Steinbaugh, M.J., Pantano, L., Kirchner, R.D., Barrera, V., Chapman, B.A., Piper, M.E., Mistry, M., Khetani, R.S., Rutherford, K.D., Hofmann, O., et al. (2018). bcbioRNASeq: R package for bcbio RNA-seq analysis [version 2; peer review: 1 approved, 1 approved with reservations]. F1000Res. *6*, 1976. 10.12688/f1000research.12093.2.

155. Patro, R., Duggal, G., Love, M.I., Irizarry, R.A., and Kingsford, C. (2017). Salmon provides fast and bias-aware quantification of transcript expression. Nat. Methods *14*, 417–419. 10.1038/nmeth.4197.

156. Soneson, C., Love, M.I., and Robinson, M.D. (2015). Differential analyses for RNA-seq: transcript-level estimates improve gene-level inferences [version 1; peer review: 2 approved]. F1000Res. *4*. 10.12688/f1000research.7563.1.

157. Love, M.I., Huber, W., and Anders, S. (2014). Moderated estimation of fold change and dispersion for RNA-seq data with DESeq2. Genome Biol. *15*, 550. 10.1186/s13059-014-0550-8.

158. Love, M.I., Anders, S., Kim, V., and Huber, W. (2016). RNA-Seq workflow: gene-level exploratory analysis and differential expression [version 2; peer review: 2 approved]. F1000Res. *4*, 1070. 10.12688/f1000research.7035.2.

159. The Gene Ontology Consortium (2019). The Gene Ontology Resource: 20 years and still GOing strong. Nucleic Acids Res. *47*, D330–D338. 10.1093/nar/gky1055.

160. Ashburner, M., Ball, C.A., Blake, J.A., Botstein, D., Butler, H., Cherry, J.M., Davis, A.P., Dolinski, K., Dwight, S.S., Eppig, J.T., et al. (2000). Gene Ontology: tool for the unification of biology. Nat. Genet. *25*, 25–29. 10.1038/75556.

161. He, L., Vanlandewijck, M., Raschperger, E., Andaloussi Mäe, M., Jung, B., Lebouvier, T., Ando, K., Hofmann, J., Keller, A., and Betsholtz, C. (2016). Analysis of the brain mural cell transcriptome. Sci. Rep. *6*, 35108. 10.1038/srep35108.